# Supplementary Information

# Binding Kinetics Survey of the Drugged Kinome.

*Victoria Georgi[1,2], Felix Schiele[†], Benedict-Tilman Berger[1,2,3], Andreas Steffen[1], Paula A. Marin Zapata[1], Hans Briem[1], Stephan Menz[1], Cornelia Preusse[1], James D.Vasta[4], Matthew B. Robers[4], Michael Brands[1], Stefan Knapp[2,3] and Amaury Fernández-Montalván[1,*]*

[1]Bayer AG, Drug Discovery, Pharmaceuticals, Müllerstr. 178, 13353 Berlin, Germany.

[2]Structural Genomics Consortium, Institute for Pharmaceutical Chemistry, Johann Wolfgang Goethe-University, Max-von-Laue-Straße 9, 60438 Frankfurt am Main, Germany.

[3]Structural Genomics Consortium, Buchmann Institute for Molecular Life Sciences, Johann Wolfgang Goethe-University, Max-von-Laue-Straße 15, 60438 Frankfurt am Main, Germany.

[4]Promega Corporation, 2800 Woods Hollow Road, Fitchburg WI 53711, USA.

*Further information and request for reagents should be directed to and will be fulfilled by Amaury Fernández-Montalván (amaury.fernandez@servier.com).

## EXPERIMENTAL PROCEDURES

### *Cell lines*

HEK-293 cells (ATCC) or HeLa cells (ATCC) were cultured in DMEM (Gibco) + 10% FBS (GE Healthcare), with incubation in a humidified, 37°C/5% CO2 incubator.

### *Plasmids*

NanoLuc tagged kinase plasmids were from Promega. For general information see [13].

### *Proteins*

Biotinylated kinases (Table S1) were purchased from Carna Biosciences. Except for His-tagged, biotinylated CDK2 and CDK9 which were synthesized in house according to previously described protocols [33,48]. In brief, human full-length CDK9 (N-terminal AviTag™ fusion protein) and cyclin T1 (N-terminal $His_6$ fusion protein) were co-expressed in Hi5 insect cells along with BirA for *in vivo* biotinylation acoording to the manufacturer (Avidity). Human full-length CDK2 (N-terminal $His_6$ and AviTag™ Fusion protein) was coexpressed in BL21(DE3) competent *E. coli* cells along with BirA. Both CDK9/cyclin T1 complexes and CDK2 were purified by immobilized metal ion affinity chromatography (HisTrap HP, GE-Healthcare).

### *Fluorescent probes and test compounds*

Alexa Fluor 647-labeled Kinase Tracers 178, 199, 222, 236, 314 and 1710 (Table S2) were obtained from Thermo Fisher Scientific. Cell permeable Kinase Tracers K-4 and K-5 were from Promega. Kinase inhibitors (Table S4) were purchased from Selleck Chemicals.

*Software and Databases*

Analysis and visualization of kinetic screening data was performed using GraphPad Prism (V.6.00-7.00), Genedata Screener ®, Biacore 4000 Evaluation Software and TIBCO Spotfire ® (V.6.5.2.). Bioinformatics analyses were conducted with Clustal Omega (https://www.ebi.ac.uk/Tools/msa/clustalo/) and Pyton 3 (http://www.pyton.org). Chemoinformatics analyses were performed with TIBCO Spotfire (V.6.5.2.) and Pipeline Pilot (Version 16.5.0.143). QSP modeling and simulations were done with Copasi 4.1.9. and Phoenix version 6.4. Figures using a phylogenetic tree of the human kinome (reproduced courtesy of Cell Signaling Technology, Inc. (www.cellsignal.com)) were prepared using the software Kinome Render (http://biophys.umontreal.ca/nrg/NRG/KinomeRender.html) and KinMap (http://kinhub.org/kinmap/). Images of kinase-inhibitor cocrystal structures were drawn with the PyMOL Molecular Graphics System (Version 1.3). Ligand interaction diagrams were generated with Discovery Studio Visualizer (v17.1.0.16143).

Information about clinical phases of kinase inhibitors was retrieved from the 1st Oncology™ database. Kinase inhibitors plasma half-lifes in healthy human adults were obtained from the Integrity℠ database. Compounds' binding mode information (including DFG- and αC-helix conformations) and kinase-ligand interaction fingerprints were from KLIFS – a structural kinase-ligand interaction database [42]. Protein crystal structures complexed to inhibitors were downloaded from the Protein Data Bank (PDB).

*Homogeneous time-resolved fluorescence resonance energy transfer (TR-FRET/HTRF) assays.*

In general, TR-FRET (HTRF) assays were conducted as described in [33]. Experiments were performed at room temperature in black 384 Well Small Volume™ HiBase Microplates (Greiner) using a buffer (50 mM Tris HCl, pH 7.5) containing 150 mM NaCl, 0.01% Tween20, 0.01% BSA and 2 mM DTT. Biotinylated kinases were incubated with 0.5 nM St-Tb (Streptavidin-Terbium (Cisbio Bioassay)) for labeling with the long-life fluorescent cryptate TR-FRET donor. Kinase Tracers 178, 199, 222, 236, 314 and 1710 served as fluorescent probes (TR-FRET acceptors). For all experiments, a nonspecific binding control (Ci) was performed in the presence of probe and 0.5 nM St-Tb, but in the absence of protein (= background signal). Fluorescence signals were detected in a PHERAstar (FS) plate reader (BMG LABTECH) by excitation of the donor with 5 laser flashes at 337 nm, followed by a time delay of 100 µs and readout of acceptor and donor emission for 400 µs at 665 and 620 nm respectively. HTRF signal (in the following often referred to as "probe binding signal") was calculated from TR-FRET Ratio values as defined in the MARS data analysis software (BMG LABTECH):

HTRF signal = TR-FRET Ratio × 10 000 = [acceptor counts / donor counts] × 10 000

*Development of equilibrium and kinetic probe competition assays (ePCA and kPCA).* For assessment of the affinity of the fluorescent probe and for determination of the optimal amount of protein for the following TR-FRET experiments, an 8-point 2-fold serial dilution of the respective Kinase Tracer (volume: 2.5 µL; final concentrations in assay: 3.125-400 nM) was incubated for at least 30 min with increasing concentrations of kinase (volume: 2.5 µL; 7-point 2-fold serial dilution; final concentrations in assay: 0.125-8 nM). The minimal amount of protein for which the signal to background ratio is around 2.5-3.5 was selected for the following TR-FRET experiments, in order to obtain a sufficiently high signal at lowest

possible target protein concentration. Tracer-kinase pairs were selected following the recommendations by the supplier. In cases where no combinations were known for a particular kinase, the above experiments were performed using all Kinase Tracers.

The steady-state affinities of probe binding to the kinases were determined by removing the baseline (subtraction of nonspecific binding control signals) and fitting of the obtained probe-target binding signals to the "One site -- specific binding" model (GraphPad Prism):

$$Y = B_{max} * X / (K_D + X)$$

Where X: concentration of probe (constrained as used in experiment); Y: specific binding signal; $B_{max}$: maximum binding signal at very high probe concentrations; $K_D$: equilibrium dissociation constant in units of X

The kinetic rate constants of fluorescent probe binding to the individual kinases, as well as the optimal assay parameters with regard to probe concentration, kinetic time intervals and duration of observation were determined in association kinetics experiments. In a typical assay 5 µL of target kinase (kinases concentrations as specified in Table S2) were added to an 8-point 2-fold serial dilution of probe (volume: 5 µL; concentrations depended on determined affinity; two or more replicates) with the reagent injectors of the plate reader followed by immediate acquisition of TR-FRET signals. Prior to and after each usage, the injectors were washed with 1 M NaOH and ddH2O. Specific signals from these association kinetics experiments were determined by removing the baseline (subtraction of nonspecific binding control signals) and globally fitted to the "Association kinetics -- two or more concentration of hot" model (GraphPad Prism):

$$K_D = k_{off} / k_{on}$$

$k_{obs} = k_{on} * L + k_{off}$

$Occupancy = L / (L + K_D)$

$Y_{max} = Occupancy * B_{max}$

$Y = Y_{max} * (1 - exp(-1 * k_{obs} * X))$

Where $K_D$: calculated equilibrium dissociation constant [M], $k_{obs}$: observed rate of probe-target complex formation, $k_{off}$: dissociation rate constant of probe [$s^{-1}$], $k_{on}$: association rate constant of probe [$M^{-1}s^{-1}$], L: probe concentration [M]; Y is the specific binding signal; $Y_{max}$ is the maximum observable signal at equilibrium; Bmax: maximum binding signal at very high probe concentrations

Using Parameter constrains: L constrained to constant values as used in experiment; Shared parameters (between concentration traces) for global fit: $k_{off}$, $k_{on}$, $B_{max}$

*Compound screening with ePCA.* Analysis of steady-state affinities of the kinase inhibitors were performed in at least two independent experiments with two duplicates each. Compounds were diluted from 10 mM DMSO stocks in Storage 384 Microplates (REMP) using the Precision$^{TM}$ Microplate Pipetting System (BioTek$^{TM}$). Serial dilutions (11-point 3.5-fold) were performed in 100% DMSO to yield 100-fold concentrated solutions that would result in final assay concentrations of 72.5 pM - 20 µM or 7.25 pM – 2 µM (depending on the inhibitor affinities) and 1% DMSO. To this end 50 nL of these stock solutions (or DMSO in control wells) were transferred from the stock plates into black 384 Well Small Volume HiBase Microplates assay plates (Greiner) using a Hummingbird Benchtop System (Digilab). The stock plates were sealed with adhesive aluminum foil by using the Quick Combi-Sealer (HJ-Bioanalytik) and stored at -20°C. The assay plates were either sealed with adhesive polypropylene foil and stored at -20°C or immediately used to run the ePCA: 3 µL of

fluorescent probe and 2 µL of target kinase (see Table S2 for kinase specific assay parameters such as probe and target concentration) were added using a Multidrop™ Combi Reagent Dispenser (Thermo Fisher Scientific) to start the competitive target kinase binding process of compound and probe. The assay was incubated for more than 1 h prior to acquisition of the TR-FRET signals. TR-FRET traces were normalized using high (100% probe binding) and low (0% probe binding = 100% inhibition) controls. These controls were calculated beforehand as mean of all signals in the respective control wells on a single microtiter plate (for 100% probe binding: wells with probe but without compound; 0% probe binding: wells with St-Tb and probe but without biotinylated kinase). Normalized data were fitted to a four-parameter sigmoidal dose-response curve using Genedata Screener™ with the proprietary automated data- and model driven outlier masking settings:

$$Y = Bottom + (Top - Bottom) / (1 + 10^{(( Log(IC_{50}) - X) * Hill\ slope)})$$

Where Y: normalized probe binding signal (response); Bottom: bottom plateau (minimal response); Top: maximum response; X: logarithms of compound concentrations; $IC_{50}$: concentration of compound required to provoke a response half way between Bottom and Top (in units of compound concentration); Hill slope: slope factor describing steepness of dose-response curve

Parameter constrains: X constrained to constant values as used in experiment; Genedata Screener software was allowed to automatically choose if to fix or not to fix the Hill slope to 1, Bottom to 0 and Top to 100, but was not allowed to extrapolate $IC_{50}$s. Thereby fixing of the parameters was enforced if the data range is <30% or $r^2 < 0.1$; If not fixed, the parameters were constrained: Hill slope must be between 0.5 and 5; Bottom must be <30%; Top must be between 70 and 150%.

The $IC_{50}$ value was converted into the equilibrium dissociation constant ($K_{D\,eq}$) by using the Cheng-Prusoff equation [49].

$$K_D = IC_{50} / (1 + L / K_{D_L})$$

Where $K_D$: equilibrium dissociation constant of compound; $IC_{50}$: concentration of compound required to provoke a response half way between minimum and maximum response; L: concentration of probe; $K_{D_L}$: equilibrium dissociation constant of probe

*Compound screening with kPCA.* Analysis of kinetic rate constants of inhibitor binding to kinases was performed in at least two independent experiments with two duplicates each. Compounds were diluted using the same instrumentation as for ePCA but with different volumes and dilution schemes. Briefly, 4-point 10-fold serial dilutions of 100x concentrated compounds were prepared in DMSO (final concentrations in assay: 2.5-2500 nM), and DMSO was applied into control wells (0% and 100% probe binding). 100 nL of these sock solutions were pre-dispensed to generate "assay-ready" plates, to which 5 µL of fluorescent probe were added prior to the experiment. To start the competitive binding assay, 5 µL of target kinase were added with the reagent injectors of the plate reader followed by immediate acquisition of TR-FRET signals (see Table S2 for kinase specific assay parameters such as probe and target concentration, measurement interval and observation time). For these experiments the script mode of the plate reader was used to dispense the target and measure plate octants as described in [33]. Prior to and after usage, the injectors were washed with 1 M NaOH and ddH2O. To determine rate constants and affinity parameters, baseline signals (0% probe binding control, assumed to be linear with time) were subtracted from the kinetic traces

(including the zero compound concentration trace = 100% probe binding control) and globally fitted to the Motulsky-Mahan's [50] "Kinetics of competitive binding" equation:

$$Y(t) = \frac{B_{max} \times K_1 \times L}{Diff}\left(\frac{K_4\ Diff}{K_F K_S} + \frac{K_4 - K_F}{K_F}\ e^{-K_F t} - \frac{K_4 - K_S}{K_S}\ e^{-K_S t}\right)$$

With

$$K_A = K_1 \times L + K_2$$

$$K_B = K_3 \times I + K_4$$

$$K_F = 0.5\ (\ K_A + K_B + \sqrt{(K_A - K_B)^2 + 4 \times K1 \times K3 \times L \times I}\ )$$

$$K_S = 0.5\ (\ K_A + K_B - \sqrt{(K_A - K_B)^2 + 4 \times K1 \times K3 \times L \times I}\ )$$

$$Diff = K_F - K_S$$

Where Y: specific probe binding signal; t: time [s]; K1: association rate of probe [$M^{-1}s^{-1}$]; K2: dissociation rate of probe [$s^{-1}$]; L: concentration of probe [M], K3: association rate of unlabeled compound [$M^{-1}s^{-1}$]; I: concentration of unlabeled compound [M]; K4: dissociation rate of unlabeled compound [$s^{-1}$]; $B_{max}$: maximum binding signal at very high concentration of probe (and often exceeds what is measured in experiment)

Parameters constrains: K1, L, K2, I constrained to constant values as used in experiment and determined during assay development. Shared parameters (between concentration traces) for global fit: K3, K4, $B_{max}$ must be greater than 0

Affinities from kinetic analysis were calculated as the ratio of the on- and off-rate:

$K_{D\,kin} = k_{off} / k_{on}$

Where $K_{Dkin}$: calculated equilibrium dissociation constant [M], $k_{off}$: dissociation rate constant [$s^{-1}$], $k_{on}$: association rate constant [$M^{-1}s^{-1}$]

Results from Monte Carlo analyses (Georgi et al. manuscript in preparation) were considered for evaluation of the data: If off-rates could not be determined accurately by nonlinear regression (if CV($k_{on} \times K_{D\,eq}$) < 50% and either case I) CV($k_{off}$) > 50% or case II) $k_{off}$ is not determinable by regression), off-rates were calculated using the equation as suggested in [33]:

$k_{off} = K_{D\,eq} \times k_{on}$

Where $K_{D\,eq}$: equilibrium dissociation constant [M] as determined in endpoint experiment ePCA, $k_{off}$: calculated dissociation rate constant in [$s^{-1}$], $k_{on}$: association rate constant [$M^{-1}s^{-1}$] as determined by using Motulsky-Mahan equation

Off-rates were set to > 0.35 (2 times faster than the fastest determined off-rate with a relative model error <40%), if CV($K_{D\,kin}$) < 50%, the difference between $K_{D\,kin}$ and $K_{D\,eq}$ is less than five-fold and kinetic rate constants ($k_{on}$, $k_{off}$) are not determinable by regression (values far beyond assay quantitation limit and/or beyond diffusion limit: $k_{on} > 10^9$ $M^{-1}s^{-1}$; $k_{off} > 10^4$ $s^{-1}$ (case III); and/or CV > 90%). Moreover, kinetic rate constants were considered as not evaluable, in all cases (which do not belong to case I-II but) with a more than five-fold difference between $K_{D\,kin}$ and $K_{D\,eq}$ (which could result from more complex interactions than simple 1:1 binding).

Residence times (RT) were calculated using the equation:

$RT = 1/k_{off}$

Where RT: residence time in units of time, $k_{off}$: dissociation rate constant in inverse time

Finally, the affinities determined with kPCA were corrected by considering the affinities determined with ePCA to derive a $K_D$ (PCA): $K_D$ (PCA) = $K_{D\ kin}$, except for the following cases: (I) $K_D$ (PCA) = $K_{D\ eq}$, if CV($K_{D\ eq}$) < 70% and 1) CV($K_{D\ kin}$) > 70% or 2) $K_{D\ kin}$ is n.e. or 3) reached assay quantitation limit or 4) there is at least a 5-fold discrepancy between $K_{D\ kin}$ and $K_{D\ eq}$; (II) else if CV($K_{D\ kin}$) and CV($K_{D\ eq}$) > 70%, but there is a less than 5-fold discrepancy between $K_{D\ kin}$ and $K_{D\ eq}$, then $K_D$ (PCA) = mean($K_{D\ kin}$, $K_{D\ eq}$).

*Cellular assay based on bioluminescence resonance energy transfer (BRET).*

The cellular NanoBRET™ Target Engagement Assays (Promega) for ABL, BTK, FYN, KIT, LCK, Ret, SRC and Tie2 were conducted according to [13]. Each kinase encoded a C-terminal fusion of NanoLuc luciferase with the exception of ABL, for which NanoLuc was at the N-terminus. In brief, cells were transiently transfected with NanoLuc / kinase fusion plasmids using FuGENE HD according to the manufacturer's protocol (Promega) and seeded at a density of 2 x $10^5$ cells per mL into white, sterile 96-well plates (Corning). 24 hours post-transfection, growth medium (90% DMEM + 10% fetal bovine serum) was replaced with Assay Medium (Opti-MEM® I Reduced Serum Medium, no phenol red). Then, 1 µL/mL of

1000x concentrated test compound was added (final concentrations: [Staurosporine]: 0.5 µM; [Imatinib]: 2 µM; [Ibrutinib], [Dasatinib], [Ponatinib]: 0.2 µM) and incubated at 37°C for 3 h. After removing unbound test compound via washout with prewarmed Assay Medium and a wash step, 100 µL Assay Medium and 1 µM (final concentration) cell-permeable fluorescent Kinase Tracer K-4 or KinaseTracer K-5 (Promega) were added, followed by immediate addition of the Complete NanoBRET™ NanoGlo® Substrate / Extracellular NanoLuc® Inhibitor Solution according to the manufacturer's protocol (Promega). Subsequently, bioluminescence resonance energy transfer was measured over 5 h in 3-minutes intervals with a GloMax® Discover Instrument equipped with NanoBRET filters. A positive control with saturating dose of kinase inhibitor (0% probe binding) served for background correction, and a probe signal control (100% probe binding) was conducted by adding only DMSO instead of compound solubilized in DMSO. For better comparability with simulated target occupancies, NanoBRET™ traces were normalized to obtain binding signals as percentage of control, according to the equation:

$$Signal_{normalized}\,(t) = (1 - (Signal\,(t) - Signal_{0\%}\,(t)) / (Signal_{100\%}\,(t) - Signal_{0\%}\,(t))) \times 100\%$$

t: time; $Signal_{0\%}$ (t): 0% probe binding signal; $Signal_{100\%}$ (t): 100% probe binding signal

Changes in cellular target occupancy (ΔTO) were calculated as follows:

$$\Delta TO_{0\text{-t min}}\,[\%] = 100 - (Signal_{normalized}\,(t) / Signal_{normalized}\,(t=0)) * 100$$

Where t: time; $Signal_{normalized}$ (t): normalized signal at time = t; $Signal_{normalized}$ (t=0): normalized signal at time = 0

Constrains for experimental traces: $Signal_{normalized}$ (t=0) was estimated based on fitting of the nomalized trace to "One phase decay" curve using GraphPad Prism. $\Delta TO_{0\text{-}t\ min}$ were set to 100% for all values >100% and to 0% for all values <0%.

Changes in simulated cellular target occupancy (see below) were calculated in the same way, but without consideration of the above mentioned constrains.

*QUANTIFICATION AND STATISTICAL METHODS*

*General statistics.*

For assessment of the direction and strength of relationship between $k_{on}$, $k_{off}$, $K_D$ values determined in different assays or replicates and their relationship with changes in cellular target occupancy (ΔTO) (using GraphPad Prism), Spearman correlation calculations were utilized to compute correlation coefficients and two-tailed P values (binding parameters are approximately log normally distributed, but skewed due to assay quantitation limits). Agreement between methods and replicates was evaluated by Bland-Altman analysis using mean log differences. Statistical analyses were performed with log values of binding parameters, including generation of histograms (bin: 0.5) and distance matrices calculations, Gini score calculation and multivariable regression analyses (for more details see below). Fitting of log values of binding parameters to a "Gaussian" curve or "Cumulative Gaussian -- Percents" curve, respectively, as well as descriptive statistics was performed using GraphPad Prism. Percent differences were calculated as defined here:

Percent difference = (value1 – value2) / (value1 + value2) * 100

*Gini scores as metric for selectivity.*

Gini scores were determined based on normalized log values of binding parameters as described by Graczyk et al. [36]. Since Gini score calculation requires values normalized between 0 and 100, log values were normalized based on minimum and maximum values.

*Plasma and dissociation half-lifes.*

Plasma half-lifes of the kinase inhibitors (applied for Fig. 3a) were calculated as median (with 25% and 75% quantil) of all entries (for our tested KI) in Integrity$^{SM}$ database for healthy human adults. The median of these plasma half-lifes was used to calculate an average elimination rate $k_{el}$ (applied for Fig. 3b): $k_{el} = \ln(2)/\text{plasma-half-life}$

*Quantitative systems pharmacology and pharmacokinetics simulations.*

Model equations for simulations of target occupancy *in vivo*

All simulations were performed until *in vivo* target occupancy traces reached equilibrium (same profile will be reached in next dosing interval).

Pharmacokinetics-binding kinetics (PK-BK) model

To simulate the compound-concentration-time profile after oral administration of a kinase inhibitor, a two-compartment model was used in Copasi 4.1.9. A simple 1:1 drug-target binding model, assuming the free drug hypotheses and constant total protein target concentrations, was added to describe compound binding to protein targets. This PK-BK model for compound binding to n proteins is given by the following equations:

PK-BK model

$$\frac{d([C_1](t))}{dt} = \frac{k_a \times A_a(t)}{V_1} - CL \times [C_1](t) - CLD \times \left([C_1](t) - [C_2](t)\right) + \sum_{i=1}^{n} \left(k_{off\,i} \times [TC]_i(t) - k_{on_i} \times \left(fu \times [C_1](t)\right) \times [T]_i(t)\right)$$

$$\frac{d([TC]_i(t))}{dt} = k_{on_i} \times \left(fu \times [C_1](t)\right) \times [T]_i(t) - k_{off\,i} \times [TC]_i(t) \qquad \text{for } i = 1,2,\ldots,n$$

$$\frac{d([C_2](t))}{dt} = CLD \times \left([C_1](t) - [C_2](t)\right)$$

$$\frac{d(A_a(t))}{dt} = -k_a \times A_a(t)$$

Target occupancies can be calculated using $TO_i(t) = [TC]_i(t) / [T_{total}]_i \times 100\%$ for i = 1,2,…,.n

Where n is the number of target kinases. The total target concentrations $[T_{total}]$ are equal to the sum of the respective free protein [T] and inhibitor-complexed protein [TC] concentrations. $k_{on}$ and $k_{off}$ represent the rate constants for association and dissociation of the compound-target complex. $[C_1]$ (= $A_1/V_1$) and $[C_2]$ (= $A_2/V_2$) are the total compound concentrations (= amount/distribution volume) in the central and peripheral compartment, respectively. $A_a$ is the amount of drug in the gastrointestinal tract (effective dose = dose × bioavailability F). fu is the unbound fraction of the compound in plasma. $k_a$, CL, CLD represent the rate constants for absorption, elimination and distribution.

The following assumptions and initial values were used for the simulations:

The total target concentrations $[T_{total}]$ were fixed to 10 nM (within the lower range of a typical concentration of signaling protein according to Milo et al. BioNumbers database [51] and as reported in literature and assumed in previous analyses [23]); [TC](t=0) = 0; A1(t=0) = A2(t=0) = 0; The model parameters $k_a$, $V_1$, $V_2$, CL and CLD were estimated on the

basis of the concentration-time profiles (using Phoenix version 6.4, Pharsight), F was fixed to 1. Administered dose, dosing interval, fu and concentration-time profiles are given in Clinical Pharmacology and Biopharmaceutics Review documents for ibrutinib (NDA: 205552) and dasatinib (NDA: 21-986; 22-072).

Pharmacokinetics and the concentration-affinity effect – PK-$K_D$ model

Steady state affinity driven compound-concentration-time profiles were simulated with the two-compartment model as described above, but without consideration of the drug-target binding model terms and the target occupancy traces were calculated using:

$$\mathrm{TO(t)} = \frac{\mathrm{fu} \times [\mathrm{C_1}](t)}{\mathrm{K_D} + \mathrm{fu} \times [\mathrm{C_1}](t)} \times 100\%.$$

Model equations for simulations of target occupancy in cells

Binding Kinetics - Permeation model

To simulate cellular target occupancy profiles in Copasi 4.1.9, a Binding Kinetics (BK) - Permeation model was developed. A simple 1:1 drug-target binding model with competition between compound and ATP was used to describe compound binding to protein targets. The total protein target concentration was assumed to be constant. Permeation of the compound trough the cellular membrane was approximated using Fick's First Law. The BK-Permeation model is given by the following equations:

BK-Permeation model

$$\frac{d([C_1](t))}{dt} = k_{off} \times [TC](t) - k_{on} \times [C_1](t) \times [T](t) - P \times A_{O,cell} \times \left([C_1](t) - [C_2](t)\right) / V_1$$

$$\frac{d([TC](t))}{dt} = k_{on} \times [C_1](t) \times [T](t) - k_{off} \times [TC](t)$$

$$\frac{d([T](t))}{dt} = k_{off} \times [TC](t) - k_{on} \times [C_1](t) \times [T](t) + k_{off,ATP} \times [T.ATP](t) - k_{on,ATP} \times [ATP](t) \times [T](t)$$

$$\frac{d([ATP](t))}{dt} = k_{off,ATP} \times [T.ATP](t) - k_{on,ATP} \times [ATP](t) \times [T](t)$$

$$\frac{d([T.ATP](t))}{dt} = k_{on,ATP} \times [ATP](t) \times [T](t) - k_{off,ATP} \times [T.ATP](t)$$

$$\frac{d([A_{2l}](t))}{dt} = P \times A_{O,cell} \times \left([C_1](t) - [C_2](t)\right)$$

Target occupancy can be calculated using $TO(t) = [TC](t) / [T_{total}] \times 100\%$

The total concentration of target protein $[T_{total}]$ is equal to the sum of free protein [T] and inhibitor-complexed protein [TC] and ATP-complexed protein [T.ATP] concentrations. $k_{on}$ and $k_{off}$ represent the rate constants for association and dissociation of the compound-target complex. [ATP] and [T.ATP] are the concentrations of ATP and ATP-complexed protein. $k_{on,ATP}$ and $k_{off,ATP}$ represent the rate constants for association and dissociation of the ATP-target complex. $[C_1](= A_1/V_1)$ and $[C_2]$ $(= A_2/V_2)$ are the compound concentrations (= amount/volume) within cells and outside cells, respectively. P is the permeability coefficient of compound through membrane. $A_{O,cell}$ is the total surface area of the cells.

The following assumptions and initial values were used for the simulations:

For simulation of the pre-incubation step (TO onset) (3h): $A_{O,cell} = 0.0154$ $dm^2$ and $V_1 = 4 \times 10^{-7}$ L (cumulated sphere surface area and volume of $2 \times 10^5$ cells); $V_2 = 0.001$ L ($2 \times 10^5$ cells / mL were applied in the nanoBRET preincubation step); $[TC](t=0) = 0$; $[T.ATP](t=0) = [ATP]/([ATP] + K_{D,ATP}) \times [T_{total}]$ (equilibrated ATP-target complex); $[T](t=0) = [T_{total}] - [T.ATP]$; $A_1(t=0) = 0$; $A_2(t=0)$ is the compound concentration applied in the experimental pre-incubation step.

For simulation of target occupancy decline after washout: [T], [TC], [T.ATP], $[C_1]$ and [ATP] at t=0 were set to the output parameters of preincubation simulations; $A_2(t=0) = 0$ (washout); $A_{O,cell} = 0.0014$ $dm^2$ and $V_1 = 3.6 \times 10^{-8}$ L (cumulated sphere surface area and volume of 18000 cells (90 µL of $2 \times 10^5$ cells / mL were applied in the washout experiment)); $V_2 = 0.0002$ L (applied assay volume).

In both parts of the simulation, the total concentration of the overexpressed target protein $[T_{total}]$ was fixed to 100 nM. ATP concentration was fixed to 0.0001 M (lower than typical cellular ATP concentrations as dead cells lose ATP [52]) or 0.001 M, respectively. ATP $k_{on}$ and $k_{off}$ were assumed to be similar for the studied kinases and were fixed to $9.2 \times 10^5$ $M^{-1}s^{-1}$ and 1.9 $s^{-1}$ [53]. Permeability coefficients (P) were set to $10^{-6}$ cm/s [54] initially, but were reduced for Imatinib ($10^{-7}$) and Ponatinib ($10^{-8}$) to simulate additional effects reducing compound intake and release. A cell size of 2000 $\mu m^3$ in volume (typical size according to Milo et al. BioNumbers database [51]) was assumed for calculation of the cumulated surface area and volume of the cells. For simulation of covalent binding of ibrutinib, the off-rate was set to $10^{-7}$ $s^{-1}$ (RT of 116 days).

Steady state affinity driven target occupancy profiles were simulated using a $K_D$-Permeation model.

$K_D$- Permeation model

The compound-concentration-time profile was simulated by:

$$\frac{d([C_1](t))}{dt} = -P \times A_{O,cell} \times \left([C_1](t) - [C_2](t)\right)/V_1$$

and $\frac{d([C_{2l}](t))}{dt} = P \times A_{O,cell} \times \left([C_1](t) - [C_2](t)\right)/V_2$

and target occupancy traces were calculated using

$$TO(t) = \frac{[C_1](t)}{K_D\left(1+\frac{[ATP](t)}{K_{D,ATP}}\right) + [C_1](t)} \times 100\%$$

Where $K_D$ represents the equilibrium dissociation constant of the compound-target complex. [ATP] and is the concentration of ATP. $K_{D,ATP}$ represents the equilibrium dissociation constant of the ATP-target complex. $[C_1](= A_1/V_1)$ and $[C_2]$ $(= A_2/V_2)$ are the compound concentrations (= amount/volume) within cells and outside cells, respectively. P is the permeability coefficient of compound through membrane. $A_{O,cell}$ is the total surface area of the cells.

Otherwise, the simulations (of pre-incubation step and target occupancy decline after washout) were conducted by using the same assumptions and initial values as described above (for the BK-Permeation model).

*Distance matrices and hierarchical clustering.*

Distance matrices were calculated as '100 minus percent similarity'.

Compound structure similarity matrix was generated with Pipeline Pilot (Version 16.5.0.143) using the component 'Fingerprint Similarity NxN' (ECFP4 fingerprint; distance measure: Tanimoto). Multiple sequence alignment of kinase constructs was performed using Clustal Omega [55].

Compound and kinase similarities were calculated with Python 3 (available at http://www.pyton.org) and the module SciPY (scipy.spatial.distance using the distance measure 'Euclidean') based on vectors of log values of binding parameters ($pK_D$, $-pk_{on}$, $pk_{off}$). No scaling or normalization was applied, on-rates and off-rates for kinase-inhibitor pairs with affinities below assay quantitation limit were set to 350 $M^{-1}s^{-1}$ and 3.5 $s^{-1}$, 'not evaluable' values were masked. In detail, Euclidean distances were calculated as follows:

$$d(f_j, f_k) = \sqrt{\sum_{i=1}^{n}(f_{j_i} - f_{k_i})^2}$$

Where for the compound-centric distance matrices: f is a feature for kinase-compound binding ($pK_D$, $-pk_{on}$ or $pk_{off}$, respectively); j is the $j^{th}$ compound; k is the $k^{th}$ compound; i is the $i^{th}$ kinase and n is the total number of kinases;

and where for the kinase-centric distance matrices: f is a feature for kinase-compound binding ($pK_D$, $-pk_{on}$ or $pk_{off}$, respectively); j is the $j^{th}$ kinase; k is the $k^{th}$ kinase; i is the $i^{th}$ compound and n is the total number of compounds.

Clustering/Visualization of distance matrices was performed with Python 3 using the modules Pandas, Seaborn and SciPY (scipy.spatial, scipy.cluster.hierarchy (routine linkage for

agglomerative clustering based on clustering method ‘average’)). Pearson correlation coefficients were used as measure for correlation between distance matrices.

*Definition and calculation of physicochemical properties of compounds.*

The molecular properties and chemical functionalities of the compounds were used as defined here: The molecular weight (MolWt) of the compounds was calculated based on the molecular formula and assuming standard isotope distribution. Flexibility is the number of rotatable bonds divided by number of bonds (between heavy atoms). Rotatable bonds are the single bonds between heavy atoms that are both not in a ring and not terminal (connected to a heavy atom which is attached to only hydrogens) as well as no amide C-N bonds. F, Cl, Br, and I atoms in a compound account for the number of halogens. The $sp^3$ C / C ratio is the number of $sp^3$ carbon atoms divided by the total number of carbon atoms. Hydrogen bond donors (HBD) are the heteroatoms (O,N,P,S) with one or more attached hydrogen atoms, while hydrogen bond acceptors (HBA) are heteroatoms (O,N,P,S) with one or more lone pairs, excluding atoms with positive formal charges, amide and pyrrole-type nitrogens, and aromatic oxygen and sulfur atoms in heterocyclic rings. The polar surface area was calculated from the molecular topology, considering all N and O atoms including attached H atoms according to Ertl [56], but excluding sulfur and phosphorus polar fragments. The prediction of predominant charge state (predominantly positive, negative or neutral molecule, based on pKa prediction) relied on Simulations Plus' ADMET predictor (v.1, 2013.0620) software. The property was applied as a qualitative variable in the analyses below and set to 1 (positive), 0 (neutral) or -1 (negative). Likewise: The compound’s binding mode information (involved subpockets and conformations, including DFG- and αC-helix conformations) and kinase-ligand interaction fingerprints (obtained from KLIFS database) are qualitative descriptors: 1

or 0 representing whether or not the kinase ligand interaction shows the respective binding feature.

*Multivariable linear regression based on a genetic function approximation algorithm.*

Multivariable linear regression models for log values of binding parameters (as dependent variable) were built with a genetic function approximation algorithm using molecular descriptors (e.g. number of HBD and HBA, $sp^3C$ / C) and/or structural features (kinase-compound interactions or binding mode information) as predictors. This was computed with Pipeline Pilot (Version 16.5.0.143) using the component 'Learn Molecular GFA Model' (for details of GFA algorithm see reference [39]) with the following parameters: population size = 100, maximum generations: 1000; initial equation length: 4, maximum equation length = 15, Scoring method: Pareto (non-dominated sorting genetic algorithm II) with Score Function: Adjusted R-squared (estimates most appropriate number of variables and penalizes overfitting).

Additionally, correlation matrices were generated with Pipeline Pilot (Version 16.5.0.143) using the component 'Correlation Matrix' calculating Pearson correlation coefficients.

SUPPLEMENTARY FIGURES

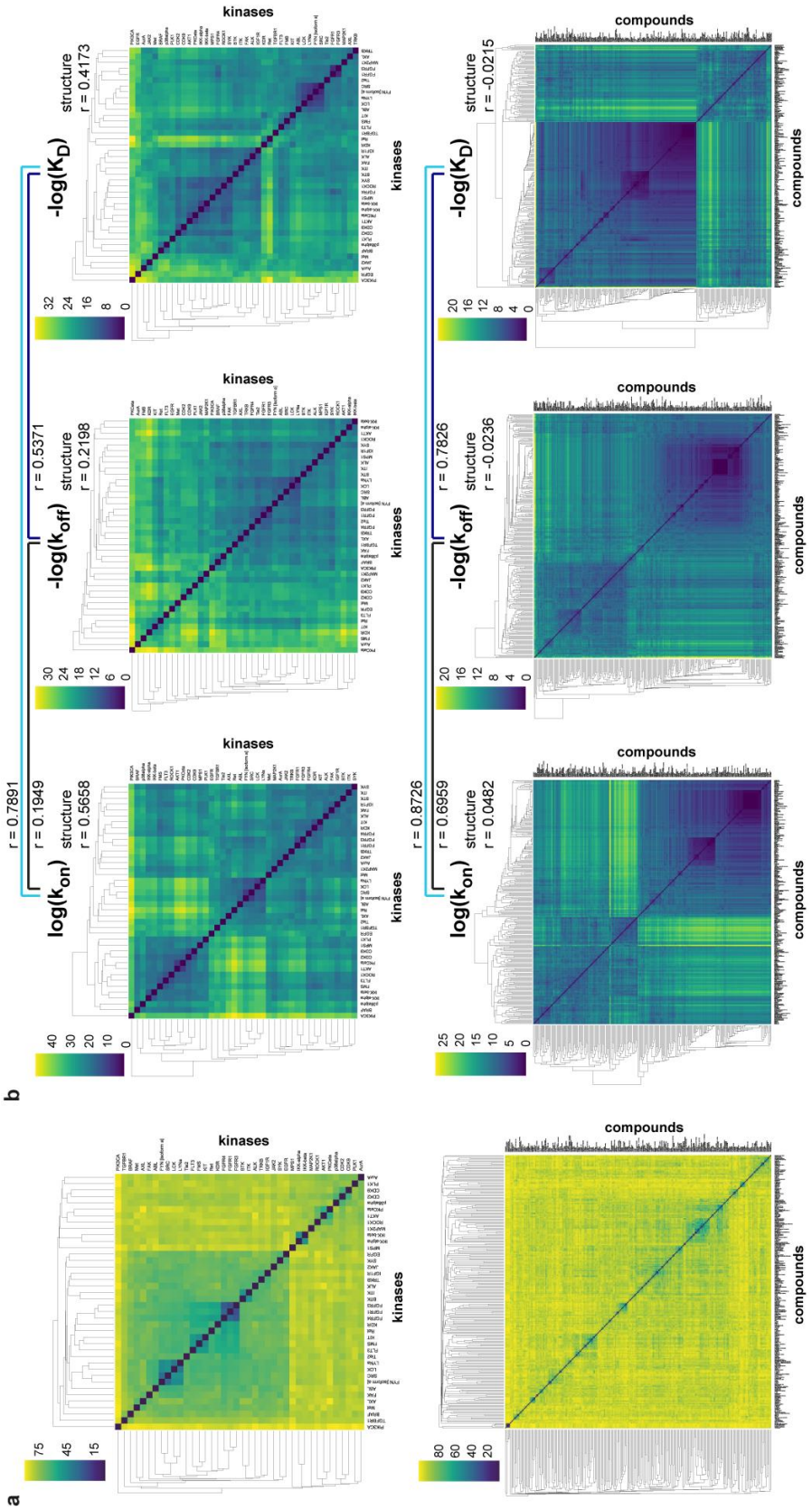


**Figure S1. Related to Figures 1 and 5. Distance matrices based on structural similarities, affinity and BK parameters per kinase (kinase-centric) and kinase inhibitor KI (compound-centric).** **(a)** Structural similarities of kinases and inhibitors investigated: Clustered Euclidean distance matrix for kinases based on sequence similarities were calculated with Clustal Omega. Clustered distance matrix for compounds are based on Tanimoto similarities of structure ECFP4 fingerprints. **(b)** Clustered distance matrices for affinity and BK parameters per kinase and KI: The colors indicate the Euclidian distances and the r values the correlation between these matrices and their correlation with the kinase sequence homology- and compound structure fingerprint-based distance matrices shown in panel a.

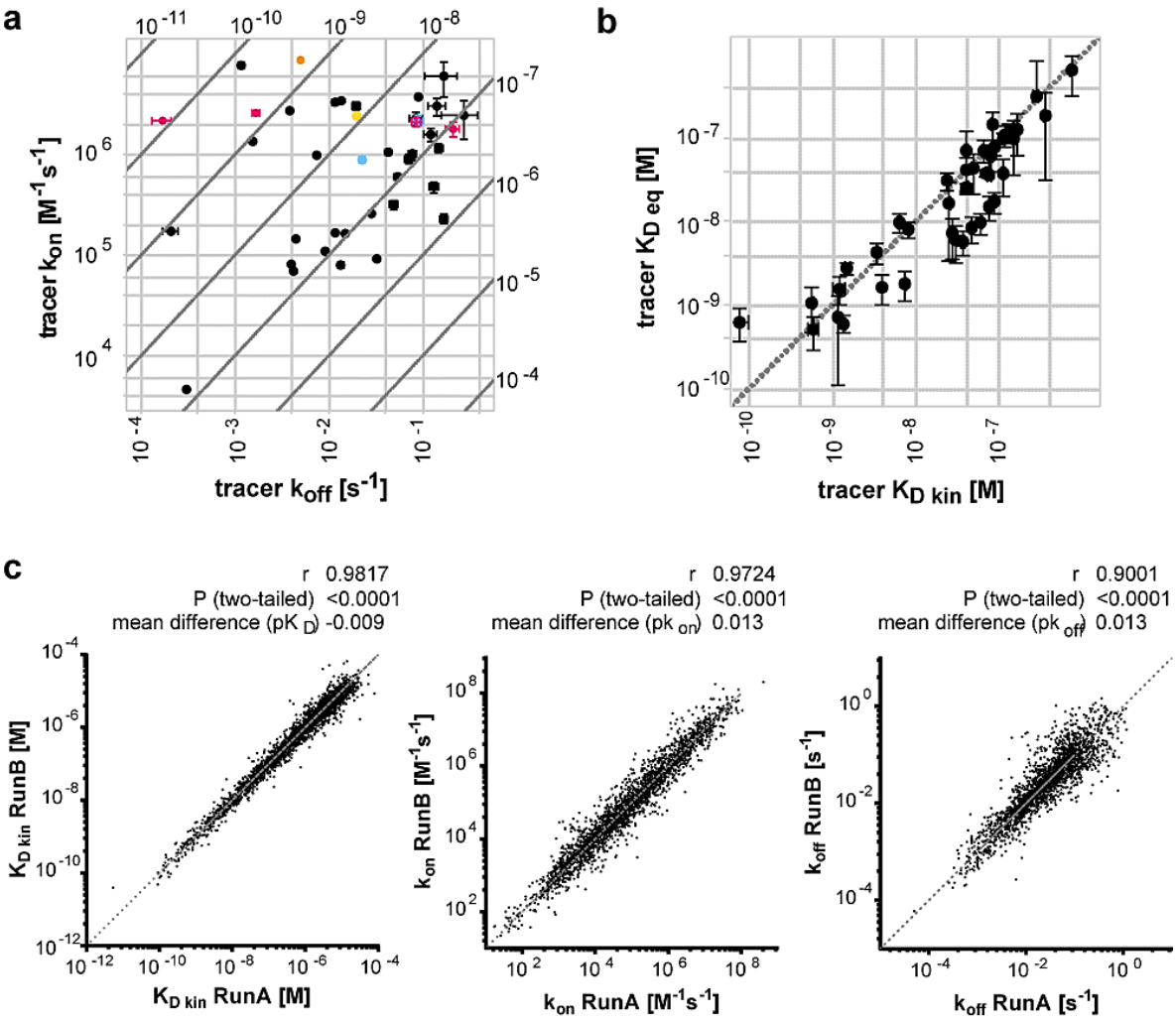


**Figure S2. Related to Figure 1. Validation of assay panel for BK profiling of KIs. (a)** Binding properties of Kinase Tracers validated in this study: RaPID plot showing BK and affinity parameters extracted from kinetic association experiments (Table S3) of the Kinase Tracers binding to 40 kinases (color code: black - Kinase Tracer 236; pink - Kinase Tracer 178; blue - Kinase Tracer 199; yellow - Kinase Tracer 222; orange - Kinase Tracer 314). **(b)** Comparison of affinities obtained from kinetic association experiments and steady state titrations of the probes. **(c)** Reproducibility of KI BK measurements performed in this study: Comparison of affinities (left panel), on-rates (middle) and off-rates (right panel) obtained in two independent runs of kPCA experiments (Run A and Run B). Statistical parameters from Spearman and Bland-Altman analyses are indicated in the graphs.

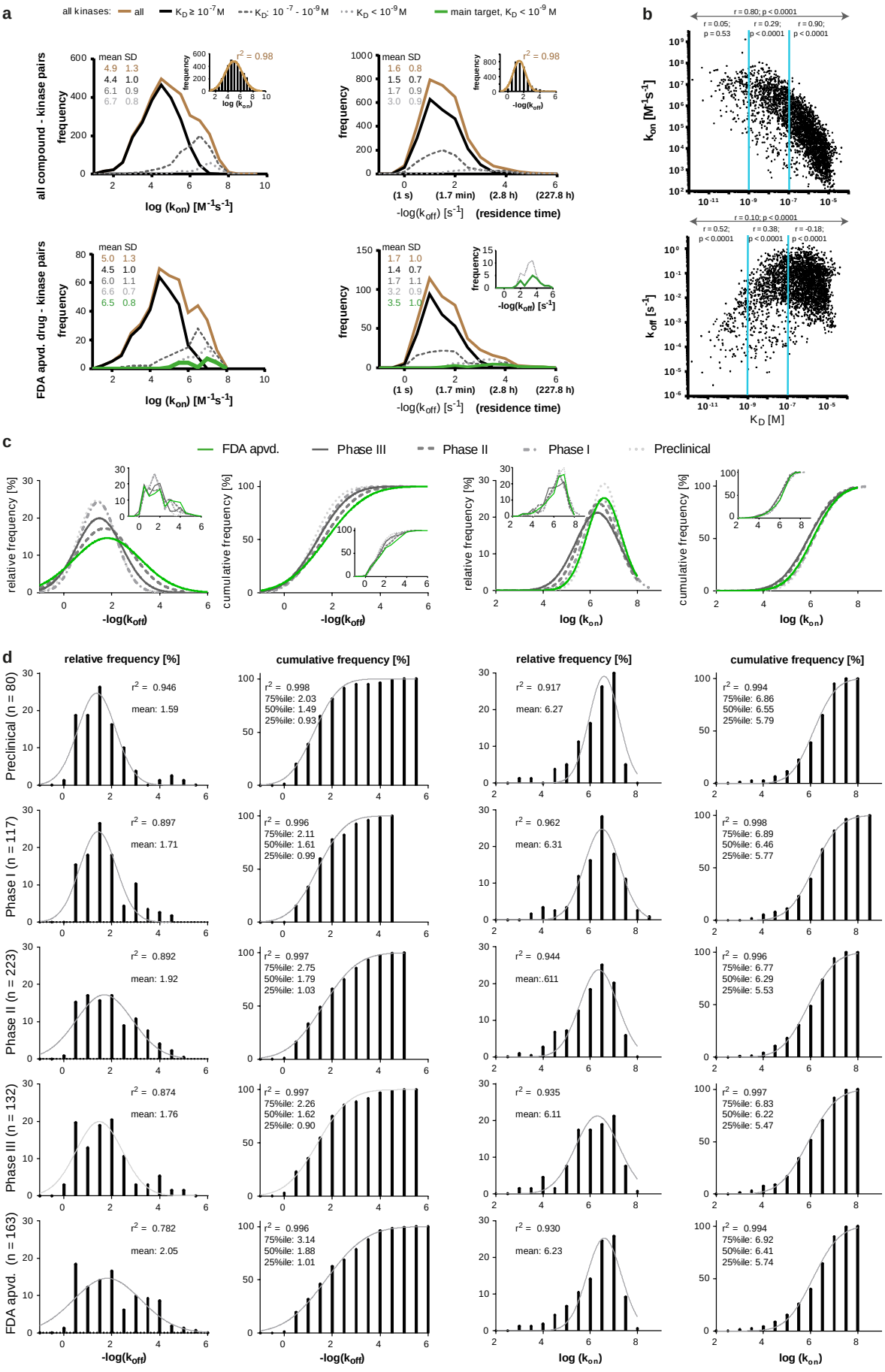
a
all kinases: all
$K_D \geq 10^{-7}$ M
$K_D$: $10^{-7}$ - $10^{-9}$ M
$K_D < 10^{-9}$ M
main target, $K_D < 10^{-9}$ M
all compound - kinase pairs
FDA apvd. drug - kinase pairs
frequency
mean SD
4.9 1.3
4.4 1.0
6.1 0.9
6.7 0.8
$r^2$ = 0.98
log ($k_{on}$) [$M^{-1}s^{-1}$]
1.6 0.8
1.5 0.7
1.7 0.9
3.0 0.9
-log($k_{off}$) [$s^{-1}$]
(1 s)
(1.7 min)
(2.8 h)
(227.8 h)
(residence time)
5.0 1.3
4.5 1.0
6.0 1.1
6.6 0.7
6.5 0.8
1.7 1.0
1.4 0.7
1.7 1.1
3.2 0.9
3.5 1.0
b
r = 0.80; p < 0.0001
r = 0.05; p = 0.53
r = 0.29; p < 0.0001
r = 0.90; p < 0.0001
$k_{on}$ [$M^{-1}s^{-1}$]
r = 0.10; p < 0.0001
r = 0.52; p < 0.0001
r = 0.38; p < 0.0001
r = -0.18; p < 0.0001
$k_{off}$ [$s^{-1}$]
$K_D$ [M]
c
FDA apvd.
Phase III
Phase II
Phase I
Preclinical
relative frequency [%]
cumulative frequency [%]
-log($k_{off}$)
log ($k_{on}$)
d
relative frequency [%]
cumulative frequency [%]
Preclinical (n = 80)
Phase I (n = 117)
Phase II (n = 223)
Phase III (n = 132)
FDA apvd. (n = 163)
$r^2$ = 0.946
mean: 1.59
$r^2$ = 0.998
75%ile: 2.03
50%ile: 1.49
25%ile: 0.93
$r^2$ = 0.917
mean: 6.27
$r^2$ = 0.994
75%ile: 6.86
50%ile: 6.55
25%ile: 5.79
$r^2$ = 0.897
mean: 1.71
$r^2$ = 0.996
75%ile: 2.11
50%ile: 1.61
25%ile: 0.99
$r^2$ = 0.962
mean: 6.31
$r^2$ = 0.998
75%ile: 6.89
50%ile: 6.46
25%ile: 5.77
$r^2$ = 0.892
mean: 1.92
$r^2$ = 0.997
75%ile: 2.75
50%ile: 1.79
25%ile: 1.03
$r^2$ = 0.944
mean:.611
$r^2$ = 0.996
75%ile: 6.77
50%ile: 6.29
25%ile: 5.53
$r^2$ = 0.874
mean: 1.76
$r^2$ = 0.997
75%ile: 2.26
50%ile: 1.62
25%ile: 0.90
$r^2$ = 0.935
mean: 6.11
$r^2$ = 0.997
75%ile: 6.83
50%ile: 6.22
25%ile: 5.47
$r^2$ = 0.782
mean: 2.05
$r^2$ = 0.996
75%ile: 3.14
50%ile: 1.88
25%ile: 1.01
$r^2$ = 0.930
mean: 6.23
$r^2$ = 0.994
75%ile: 6.92
50%ile: 6.41
25%ile: 5.74

**Figure S3. Related to Figure 2. Distribution of BK parameters quantified in this study (3230) and its dependence on the clinical phase of the KI. (a)** Histograms (Frecuency = No. of values) showing on- and off-rates distributions (left and right panels respectively) depending on the affinities of all kinase-inhibitor pairs (top) and those approved by the FDA (bottom). To ease visualization, bins are omitted and histograms are displayed as curves connecting frequency values of adjacent bins. The insets in the top panels represent histograms for all kinase-inhibitor pairs and the corresponding fits to the Gaussian distribution (as solid lines). **(b)** Comparison of all on- and off-rates (top and bottom panels respectively) to the compound affinities measured. Only parameters within assay detection limits are shown. Spearman correlation statistics for the complete dataset and three affinity groups (indicated by cyan lines) are indicated on top of the graphs. **(c-d)** Relative and cumulative frequency distributions of rate constants among KIs' from different phases in the pharmaceutical development pipeline: Distribution histograms corresponding to off-rates (first two panels from left) and on-rates (third and fourth panels from left) for all interactions with $K_D < 10^{-7}$ M grouped by inhibitors' clinical development status. Relative frequency distributions are shown in the first and third panels and cumulative frequency distributions in the second and fourth panels. Panel **(c)** shows all fits to the Gaussian distribution. The corresponding raw data histograms are shown as insets (To ease visualization, bins are omitted and histograms are displayed as curves connecting frequency values of adjacent bins). **(d)** Histograms (bars) and fits to the Gaussian distribution (solid lines) for the compounds whose BK could be quantified in this study. Descriptive statistics values are indicated in the graphs.

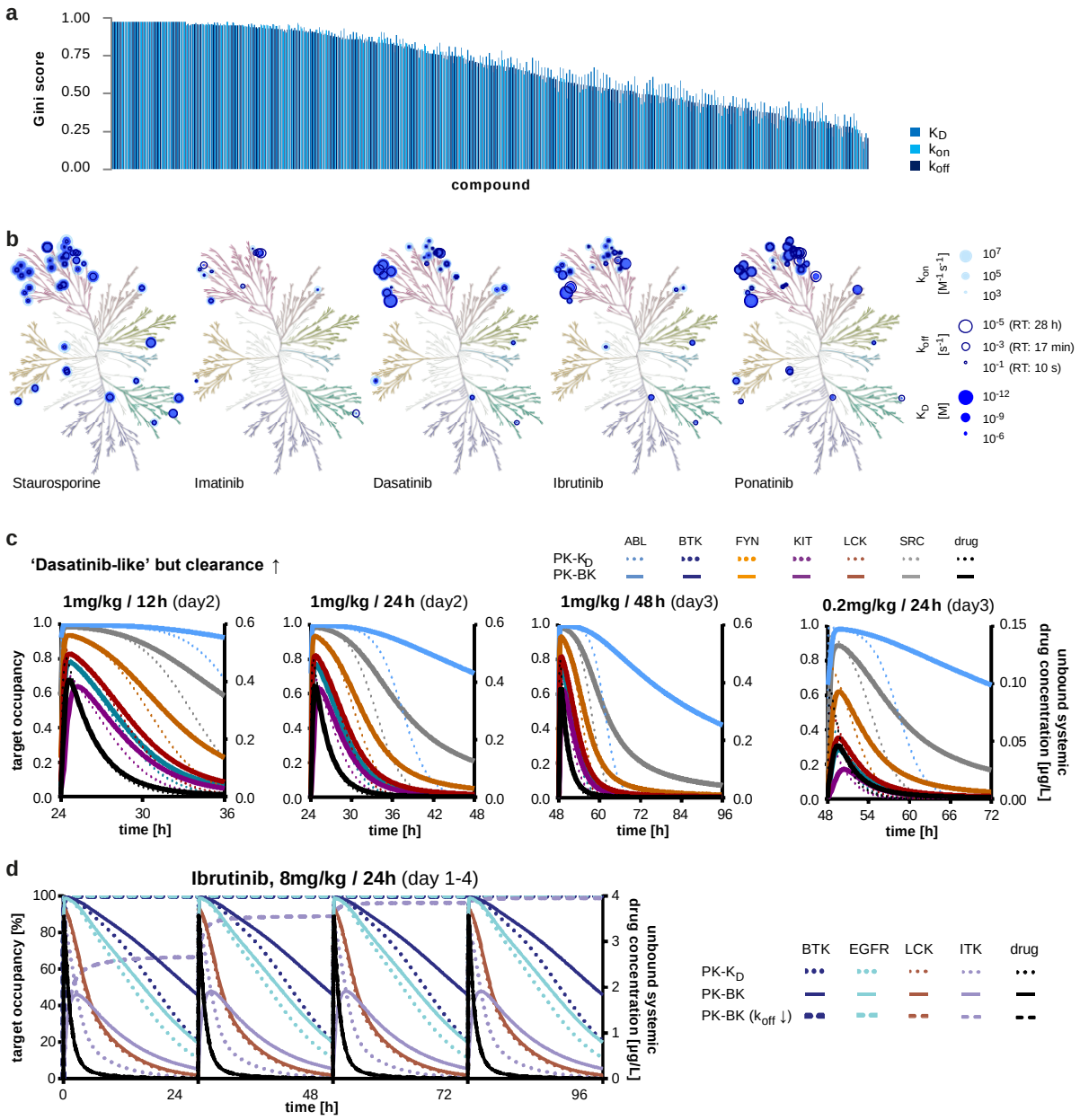


**Figure S4. Related to Figure 3. Assessment of KI kinetic selectivity with classic *vs.* new approaches. (a)** Overall selectivity of KIs evaluated in this study (with methods designed to analyze steady state binding data): Gini selectivity scores of all KIs based on their affinities, on-rates or off-rates. **(b)** Phylogenetic trees representing the human kinome and the binding of five KIs. The symbol colors represent the individual binding parameters measured and their size their magnitude. **(c-d)** QSP simulations of dynamic target occupancy by KI *in vivo*: **(c)** Simulations of the time course of *in vivo* TO by a hypothetical 'Dasatinib-like' compound with a faster clearance (4-fold intercompartmental clearance; 10-fold plasma clearance) but otherwise identical BK and PK parameters as the KI Dasatinib, from the binding kinetics (PK-BK) and affinity (PK-$K_D$) perspectives. Longer dosing intervals lead to higher discrepancies between the models (indicating hysteresis), but also to lower target occupancies at the end of the dosing interval in the PK-BK model. A lower dose (right panel) leads to lower maximum target occupancies, especially in the PK-BK model. (Day: day where target occupancy traces reached equilibrium). **(d)** Ibrutinibs main target BTK and three off-targets (EGFR, LCK and ITK) were followed using three models: one in which TO is driven by steady state affinity

(PK-$K_D$), a second one assuming BK for a 1:1 reversible interaction (PK-BK), and a third one considering covalent inhibition of BTK, EGFR and ITK (PK-BK ($k_{off}\downarrow$)). Current clinical dosage and administration schedules were used.

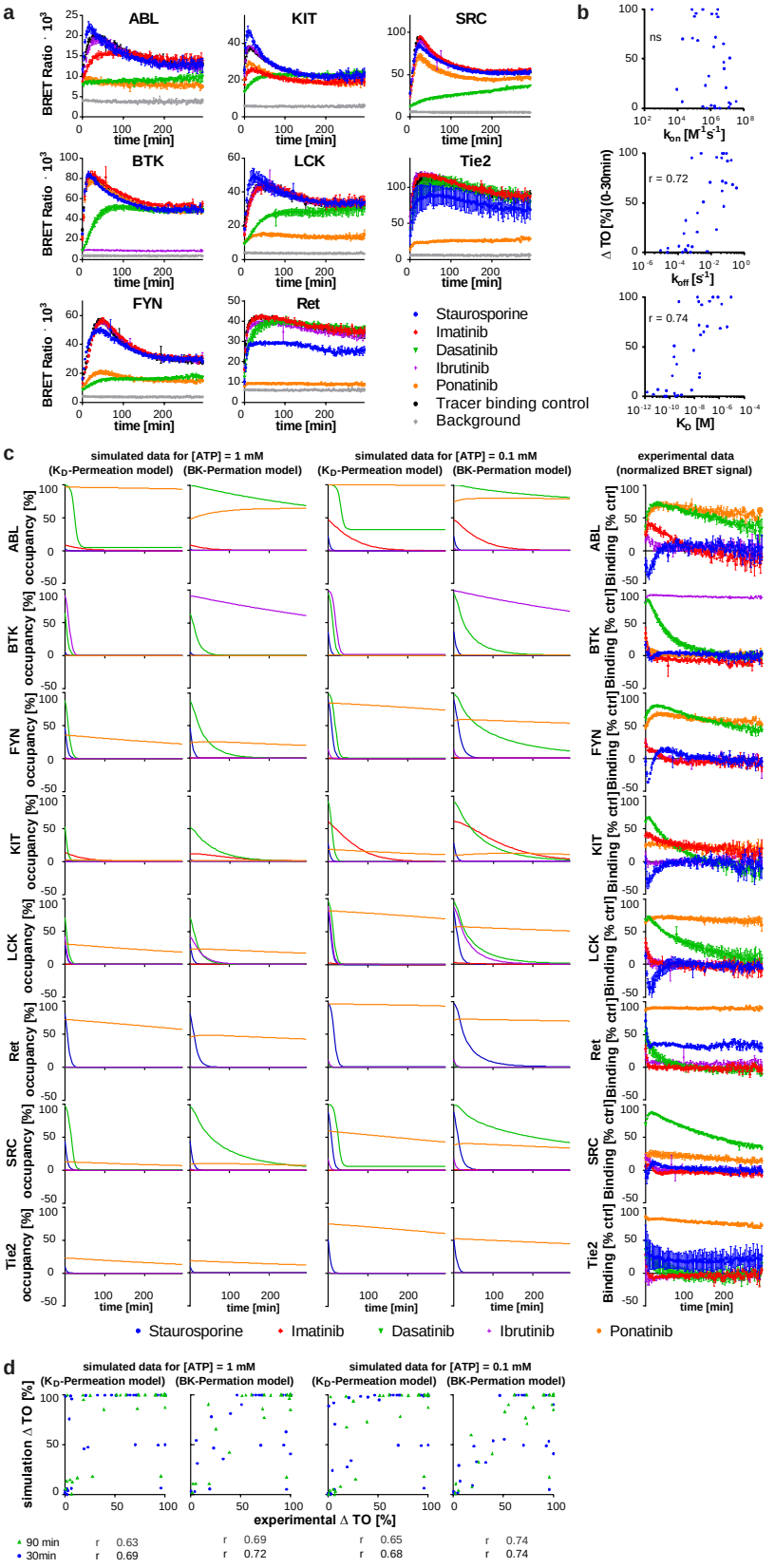


**Figure S5. Related to Figure 4. Translation of biochemical BK parameters to dynamic TO in cells (full dataset).**
**(a)** NanoBRET™ assays for dynamic target engagement by KIs in intact cells: Time courses of NanoBRET™ probe binding to eight RTKs in intact cells after treatment with six KIs or DMSO, followed by drug washout. **(b)** Comparison of the on-rates, off-rates or affinities for kinase-inhibitor pairs with percent changes in TO (ΔTO) during the first 30 minutes after washout (as measure for intracellular target engagement). Correlation coefficients are indicated in the graphs (n.s. if analysis not significant). **(c)** Simulated time course of TO decline upon compound washout using equilibrium affinity ($K_D$)-based (column 1, 3) or BK-based (column 2, 4) permeation models and either assuming 1 mM ATP (column 1-2) or 0.1 mM ATP (column 3-4), compared to normalized experimental data from NanoBRET™ washout experiments (right column) shown in panel a. **(d)** Comparison between simulated and experimental traces by using percent changes in TO (ΔTO) during the first 30 and 90 minutes after washout.

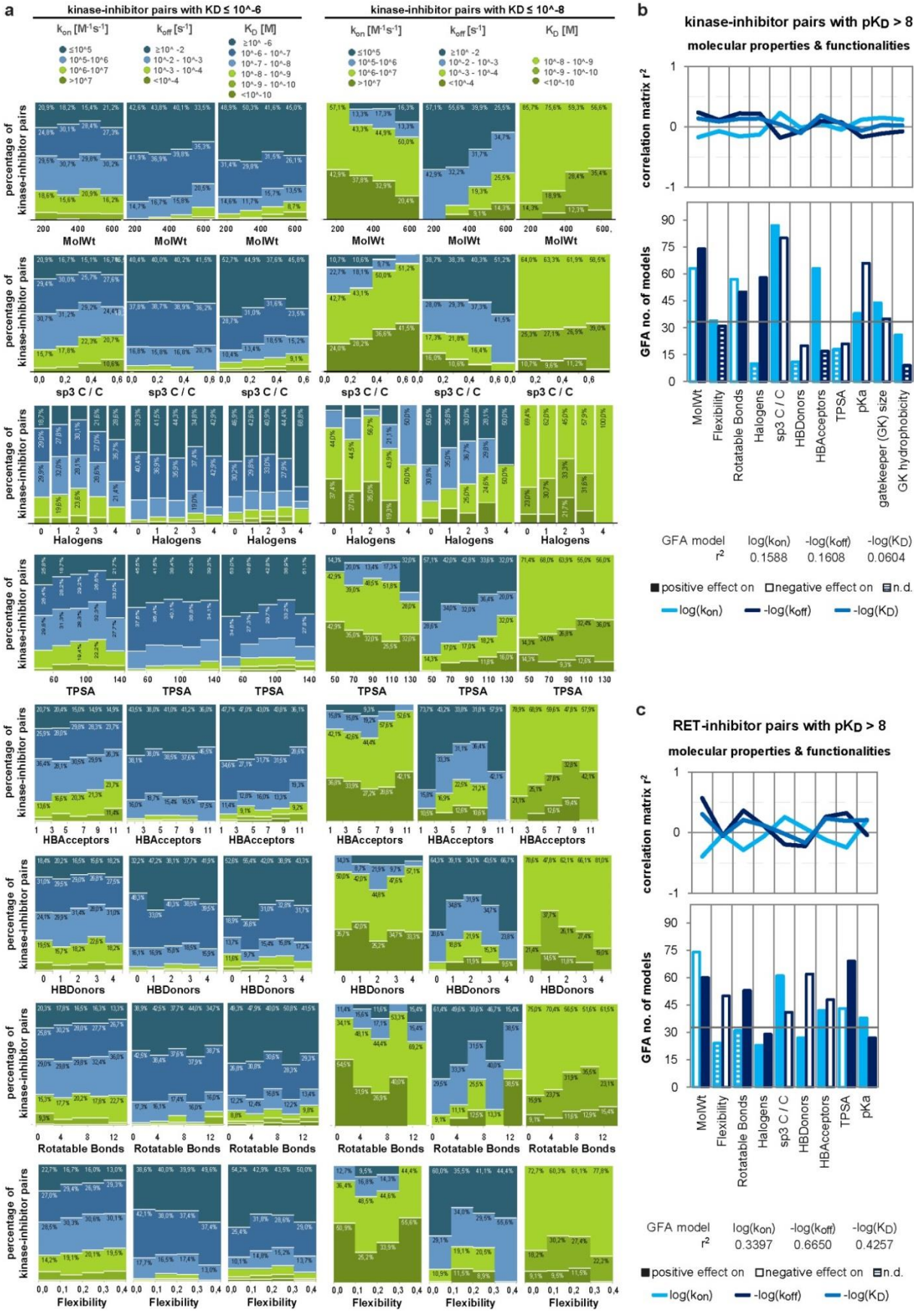
a
kinase-inhibitor pairs with KD ≤ 10^-6
kinase-inhibitor pairs with KD ≤ 10^-8
kon [M-1s-1]
koff [s-1]
KD [M]
percentage of kinase-inhibitor pairs
MolWt
sp3 C / C
Halogens
TPSA
HBAcceptors
HBDonors
Rotatable Bonds
Flexibility
b
kinase-inhibitor pairs with pKD > 8
molecular properties & functionalities
correlation matrix r²
GFA no. of models
MolWt
Flexibility
Rotatable Bonds
Halogens
sp3 C / C
HBDonors
HBAcceptors
TPSA
pKa
gatekeeper (GK) size
GK hydrophobicity
GFA model
log(kon)
-log(koff)
-log(KD)
r²
0.1588
0.1608
0.0604
positive effect on
negative effect on
n.d.
log(kon)
-log(koff)
-log(KD)
c
RET-inhibitor pairs with pKD > 8
molecular properties & functionalities
correlation matrix r²
GFA no. of models
GFA model
log(kon)
-log(koff)
-log(KD)
r²
0.3397
0.6650
0.4257
positive effect on
negative effect on
n.d.
log(kon)
-log(koff)
-log(KD)

**Figure S6. Related to Figure 5. Compound properties influencing affinity and BK parameters. (a)** The bar charts represent relative (percentage) on-, off-rates and affinity distributions for KI pairs with $K_D \leq 10^{-6}$ M (left panel) or $K_D \leq 10^{-8}$ M (right panel). Each row show a different compound molecular property **(b)** Relationships between BK parameters and molecular properties (for kinase-inhibitor pairs with $K_D \leq 10^{-8}$ M) found with genetic function approximation (GFA). Line plots and bar charts represent exemplary results of correlation analyses ($r^2$) and multivariable linear regression models built (number of variable usage in GFA models) respectively. **(c)** Same analysis was conducted for the RTK Ret only. The higher $r^2$ values support the potential utility of this type of analysis in SKR studies focusing on a single target.

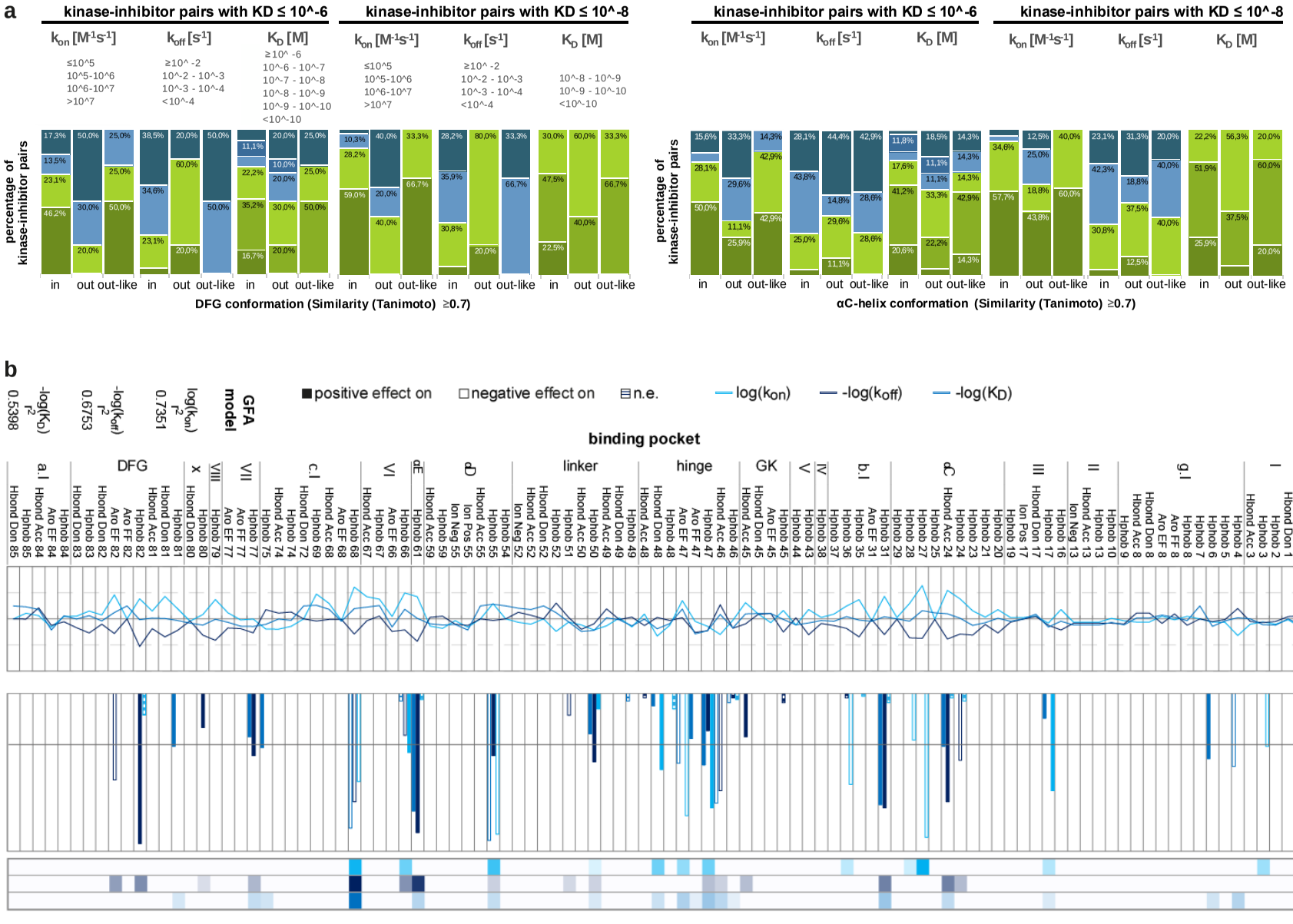
a
kinase-inhibitor pairs with KD ≤ 10^-6
kinase-inhibitor pairs with KD ≤ 10^-8
kon [M-1s-1]
koff [s-1]
KD [M]
≤10^5
10^5-10^6
10^6-10^7
>10^7
≥10^ -2
10^-2 - 10^-3
10^-3 - 10^-4
<10^-4
≥10^ -6
10^-6 - 10^-7
10^-7 - 10^-8
10^-8 - 10^-9
10^-9 - 10^-10
<10^-10
10^-8 - 10^-9
10^-9 - 10^-10
<10^-10
percentage of kinase-inhibitor pairs
in
out
out-like
DFG conformation (Similarity (Tanimoto) ≥0.7)
αC-helix conformation (Similarity (Tanimoto) ≥0.7)
b
GFA model
-log(KD) r2 0.5398
-log(koff) r2 0.6753
log(kon) r2 0.7351
positive effect on
negative effect on
n.e.
log(kon)
-log(koff)
-log(KD)
binding pocket
a.l
DFG
x
VIII
VII
c.l
VI
αE
αD
linker
hinge
GK
V
IV
b.l
αC
III
II
g.l
I
correlation matrix r2
GFA no. of models
GFA coefficient
kon
koff
KD

**Figure S7. Related to Figure 6. Effect of KI pose and structural features of kinase-inhibitor complexes on affinity and BK parameters. (a)** The bar charts represent relative (percentage) on-, off-rates and affinity distributions for kinase-inhibitor pairs with $K_D \leq 10^{-6}$ M or $K_D \leq 10^{-8}$ M. Bottom and top panels show different KI pose (i.e. kinase conformation as specified in KLIFs database for kinase-inhibitor pairs with PDB entry). **(b)** 85 binding site residues specified in the KLIFs database were investigated using correlation analyses and multivariable linear regression models built by genetic function approximation (considering only kinase-inhibitor pairs with PDB and KLIFS entry). The goal was to explore the relationships between specific interactions of the compounds and their binding properties ($k_{on}$, $k_{off}$, $K_D$). Correlation matrix $r^2$ values are shown as line plot (left), number of variable usage in models built by GFA are represented as bar chart (middle), and mean GFA coefficients for individual binding parameters are displayed as heatmap (right).The graphs shows all interactions which are different for at least two kinase-inhibitor pairs.

SUPPLEMENTARY TABLES

**Table S1. Related to Figures 1 and S1:** Kinase constructs used in this study

| Kinase | Gene ID | UniProt | Amino acids | Main target of FDA–approved drug screened in this study after [1] |
|---|---|---|---|---|
| **ABL** | 25 | P00519 | Full-length 2-1130 | Bosutinib, Dasatinib, Imatinib, Nilotinib, Ponatinib |
| **AKT1** | 207 | P31749 | catalytic domain 104-480 | |
| **ALK** | 238 | Q9UM73 | cytoplasmic domain 1058-1620 | CH5424802 (Alectinib), Crizotinib |
| **AurA** | 6790 | O14965 | Full-length 1-403 | |
| **AXL** | 558 | P30530 | cytoplasmic domain 464-885 | |
| **BRAF** | 673 | P15056 | catalytic domain 433-726 | Dabrafenib, Vemurafenib |
| **BTK*** | 695 | Q06187 | Full-length 2-659 | Ibrutinib |
| **CDK2** | 1017 | P24941 | Full-length 1-298 | |
| **CDK9** | 1025 | P50750 | Full-length | |
| **CHK1** | 1111 | O14757 | Full-length 1-476 | |
| **EGFR** | 1956 | P00533 | cytoplasmic domain 669-1210 | Afatinib, Vargatef (Nintedanib), Desmethyl Erlotinib, Gefitinib, Lapatinib, Vandetanib |
| **FAK** | 5747 | Q05397 | Truncated 376-1052 | |
| **FGFR1*** | 2260 | P11362 | cytoplasmic domain 398-822 | |
| **FGFR3*** | 2261 | P22607 | cytoplasmic domain 436-806 | |
| **FGFR4** | 2264 | P22455 | cytoplasmic domain 460-802 | |
| **FLT3** | 2322 | P36888 | cytoplasmic domain 564-993 | |
| **FMS** | 1436 | P07333 | cytoplasmic domain 538-972 | |
| **FYN [isoform a]** | 2534 | P06241 | Full-length 1-537 | |
| **IGF1R*** | 3480 | P08069 | cytoplasmic domain 959-1367 | |
| **IKK-alpha** | 1147 | O15111 | Full-length 1-745 | |
| **IKK-beta** | 3551 | O14920 | Truncated 1-662 | |
| **ITK*** | 3702 | Q08881 | Full-length 2-620 | |
| **JAK2** | 3717 | O60674 | catalytic domain 826-1132 | Ruxolitinib, Tofacitinib |
| **KDR** | 3791 | P35968 | cytoplasmic domain 790-1356 | Apatinib, Axitinib, Vargatef (Nintedanib), Lenvatinib, Pazopanib, Sunitinib, Vandetanib, Cabozantinib |
| **KIT*** | 3815 | P10721 | cytoplasmic domain 544-976 | Axitinb, Imatinib, Nilotinib, Pazopanib, Sunitinib |
| **LCK** | 3932 | P06239 | Full-length human 1-509 | |
| **LYNa** | 4067 | P07948 | Full-length1-512 | |
| **MAP2K1** | 5604 | Q02750 | Full-length 1-393 | Selumetinib, Trametinib |
| **Met** | 4233 | P08581 | cytoplasmic domain 956-1390 | Crizotinib, Cabozantinib |
| **MPS1 (TTK)** | 7272 | P33981 | Full-length 1-857 | |
| **p38alpha**** | 1432 | Q16539 | Truncated 9-352 | |
| **PIK3CA***** | 5290 | P42336 | Full-length1-1068 | |
| **PKCeta** | 5583 | P24723 | Full-length human 1-683 | |
| **PLK1** | 5347 | P53350 | Full-length1-603 | |
| **Ret** | 5979 | P07949 | cytoplasmic domain 658-1114 | Sunitinib |
| **ROCK1** | 6093 | Q13464 | catalytic domain 1-477 | |
| **SRC** | 6714 | P12931 | Full-length 1-536 | Bosutinib, Dasatinib |
| **SYK*** | 6850 | P43405 | Full-length 1-635 | |
| **TGFBR1** | 7046 | P36897 | catalytic domain 200-503 | |
| **Tie2*** | 7010 | Q02763 | cytoplasmic domain 771-1124 | |
| **TRKB*** | 4915 | Q16620 | cytoplasmic domain 456-822 | |

*preactivated with ATP treatment, **co-expression with NP_002749.2 and NP_002410.1, ***co-expression with NP_852664.1

**Table S2. Related to Figures 1, S2 and Supplementary Spreadsheet:** Assay conditions for ePCA and kPCA

| | Probe | Probe conc. [nM] | Kinase conc. [nM] | Kinetic intervals [s]* |
|---|---|---|---|---|
| **ABL** | Tracer 178 | 10 | 0.1 | 10 |
| **AKT1** | Tracer 236 | 50 | 0.5 | 10 |
| **ALK** | Tracer 236 | 10 | 0.5 | 10 |
| **AURA** | Tracer 236 | 12.5 | 0.3 | 10 |
| **AXL** | Tracer 236 | 25 | 0.2 | 10 |
| **BRAF** | Tracer 178 | 125 (kPCA), 50 (ePCA) | 2 | 10 |
| **BTK** | Tracer 178 | 12.5 | 0.2 | 10 |
| **CDK2** | Tracer 236 | 200 | 2.0 | 10 |
| **CDK9** | Tracer 236 | 200 (kPCA), 50 (ePCA) | 1 | 10 |
| **CHK1** | Tracer 236 | 400 | 2.0 | 10 |
| **EGFR** | Tracer 199 | 25 | 0.5 | 10 |
| **FAK** | Tracer 236 | 25 | 0.3 | 10 |
| **FGFR1** | Tracer 236 | 50 | 0.3 | 10 |
| **FGFR3** | Tracer 236 | 50 | 0.3 | 10 |
| **FGFR4** | Tracer 236 | 120 | 0.4 | 10 |
| **FLT3** | Tracer 236 | 50 | 0.3 | 10 |
| **FMS** | Tracer 236 | 100 | 0.5 | 10 |
| **Fyn** | Tracer 236 | 50 | 0.2 | 10 |
| **IGF1R** | Tracer 236 | 100 | 1.0 | 10 |
| **IKK-α** | Tracer 236 | 70 | 2.0 | 10 |
| **IKK-β** | Tracer 236 | 100 | 0.5 | 10 |
| **ITK** | Tracer 236 | 50 | 1.0 | 10 |
| **JAK2** | Tracer 236 | 5 | 0.4 | 10 |
| **KDR** | Tracer 236 | 50 | 0.3 | 10 |
| **KIT** | Tracer 222 | 12.5 | 0.3 | 10 |
| **LCK** | Tracer 236 | 50 | 0.3 | 10 |
| **LYN A** | Tracer 236 | 25 | 0.3 | 10 |
| **MAP2K1** | Tracer 236 | 25 | 0.1 | 10 |
| **MET** | Tracer 236 | 50 | 0.2 | 10 |
| **MPS1** | Tracer 236 | 250 (kPCA), 50 (ePCA) | 1 | 10 |
| **p38a** | Tracer 199 | 50 | 0.124 | 10 |
| **PIK3CA** | Tracer 314 | 5 | 0.121 | 10 |
| **PKCη** | Tracer 236 | 100 | 0.4 | 120 |
| **PLK1** | Tracer 236 | 50 | 4.0 | 10 |
| **RET** | Tracer 236 | 25 | 0.3 | 10 |
| **ROCK1** | Tracer 236 | 200 | 1.0 | 10 |
| **SRC** | Tracer 236 | 25 | 0.3 | 10 |
| **Syk** | Tracer 236 | 5 | 0.2 | 10 |
| **TGF-β1** | Tracer 178 | 25 | 0.3 | 10 |
| **TIE2** | Tracer 236 | 50 | 0.3 | 10 |
| **TRKB** | Tracer 236 | 25 | 0.2 | 10 |

* Further reader settings: excitation - 337 nm / emission - A: 665 nm, B: 620 nm / 40 cycles

**Table S3. Related to Figures 1 and S2:** Binding kinetic and affinity parameters of kPCA probes

| | $k_{on}$ [$M^{-1}s^{-1}$] | | $k_{off}$ [$s^{-1}$] | | $K_{D\ kin}$ [M] | |
|---|---|---|---|---|---|---|
| | mean | error | mean | error | mean | error |
| **ABL** | $\mathbf{2.19 \cdot 10^{6}}$ | $1.95 \cdot 10^{4}$ | $\mathbf{1.70 \cdot 10^{-4}}$ | $4.00 \cdot 10^{-5}$ | $\mathbf{8.00 \cdot 10^{-11}}$ | $2.00 \cdot 10^{-11}$ |
| **AKT1** | $\mathbf{8.09 \cdot 10^{4}}$ | $1.15 \cdot 10^{3}$ | $\mathbf{3.99 \cdot 10^{-3}}$ | $9.00 \cdot 10^{-5}$ | $\mathbf{4.93 \cdot 10^{-8}}$ | $1.18 \cdot 10^{-9}$ |
| **ALK** | $\mathbf{3.75 \cdot 10^{6}}$ | $2.18 \cdot 10^{5}$ | $\mathbf{9.02 \cdot 10^{-2}}$ | $5.33 \cdot 10^{-3}$ | $\mathbf{2.41 \cdot 10^{-8}}$ | $2.30 \cdot 10^{-10}$ |
| **AURA** | $\mathbf{1.34 \cdot 10^{6}}$ | $1.50 \cdot 10^{4}$ | $\mathbf{1.55 \cdot 10^{-3}}$ | $6.00 \cdot 10^{-5}$ | $\mathbf{1.16 \cdot 10^{-9}}$ | $4.00 \cdot 10^{-11}$ |
| **AXL** | $\mathbf{3.31 \cdot 10^{6}}$ | $1.59 \cdot 10^{5}$ | $\mathbf{1.17 \cdot 10^{-2}}$ | $8.10 \cdot 10^{-4}$ | $\mathbf{3.52 \cdot 10^{-9}}$ | $1.30 \cdot 10^{-10}$ |
| **BRAF** | $\mathbf{1.79 \cdot 10^{6}}$ | $3.04 \cdot 10^{5}$ | $\mathbf{2.11 \cdot 10^{-1}}$ | $3.58 \cdot 10^{-2}$ | $\mathbf{1.18 \cdot 10^{-7}}$ | $1.93 \cdot 10^{-9}$ |
| **BTK** | $\mathbf{2.56 \cdot 10^{6}}$ | $5.20 \cdot 10^{4}$ | $\mathbf{1.67 \cdot 10^{-3}}$ | $1.60 \cdot 10^{-4}$ | $\mathbf{6.10 \cdot 10^{-10}}$ | $8.00 \cdot 10^{-11}$ |
| **CDK2** | $\mathbf{7.94 \cdot 10^{4}}$ | $4.46 \cdot 10^{3}$ | $\mathbf{1.35 \cdot 10^{-2}}$ | $8.70 \cdot 10^{-4}$ | $\mathbf{1.70 \cdot 10^{-7}}$ | $5.85 \cdot 10^{-9}$ |
| **CDK9** | $\mathbf{1.67 \cdot 10^{5}}$ | $4.30 \cdot 10^{3}$ | $\mathbf{1.17 \cdot 10^{-2}}$ | $2.27 \cdot 10^{-4}$ | $\mathbf{7.01 \cdot 10^{-8}}$ | $1.85 \cdot 10^{-9}$ |
| **CHK1** | $\mathbf{2.75 \cdot 10^{4}}$ | $1.34 \cdot 10^{3}$ | $\mathbf{4.53 \cdot 10^{-3}}$ | $3.40 \cdot 10^{-4}$ | $\mathbf{1.65 \cdot 10^{-7}}$ | $1.19 \cdot 10^{-8}$ |
| **EGFR** | $\mathbf{8.90 \cdot 10^{5}}$ | $5.12 \cdot 10^{4}$ | $\mathbf{2.25 \cdot 10^{-2}}$ | $1.40 \cdot 10^{-3}$ | $\mathbf{2.53 \cdot 10^{-8}}$ | $5.80 \cdot 10^{-10}$ |
| **FAK** | $\mathbf{1.05 \cdot 10^{6}}$ | $5.32 \cdot 10^{4}$ | $\mathbf{4.27 \cdot 10^{-2}}$ | $2.66 \cdot 10^{-3}$ | $\mathbf{4.06 \cdot 10^{-8}}$ | $1.45 \cdot 10^{-9}$ |
| **FGFR1** | $\mathbf{9.05 \cdot 10^{5}}$ | $9.88 \cdot 10^{4}$ | $\mathbf{7.24 \cdot 10^{-2}}$ | $8.81 \cdot 10^{-3}$ | $\mathbf{8.00 \cdot 10^{-8}}$ | $3.78 \cdot 10^{-9}$ |
| **FGFR3** | $\mathbf{5.97 \cdot 10^{5}}$ | $3.95 \cdot 10^{4}$ | $\mathbf{5.37 \cdot 10^{-2}}$ | $4.15 \cdot 10^{-3}$ | $\mathbf{8.99 \cdot 10^{-8}}$ | $3.56 \cdot 10^{-9}$ |
| **FGFR4** | $\mathbf{2.29 \cdot 10^{5}}$ | $2.29 \cdot 10^{4}$ | $\mathbf{1.69 \cdot 10^{-1}}$ | $1.67 \cdot 10^{-2}$ | $\mathbf{7.37 \cdot 10^{-7}}$ | $2.20 \cdot 10^{-8}$ |
| **FLT3** | $\mathbf{6.89 \cdot 10^{4}}$ | $6.84 \cdot 10^{2}$ | $\mathbf{4.23 \cdot 10^{-3}}$ | $7.00 \cdot 10^{-5}$ | $\mathbf{6.15 \cdot 10^{-8}}$ | $9.10 \cdot 10^{-10}$ |
| **FMS** | $\mathbf{1.10 \cdot 10^{5}}$ | $3.30 \cdot 10^{3}$ | $\mathbf{9.21 \cdot 10^{-3}}$ | $3.40 \cdot 10^{-4}$ | $\mathbf{8.38 \cdot 10^{-8}}$ | $1.94 \cdot 10^{-9}$ |
| **Fyn** | $\mathbf{3.00 \cdot 10^{6}}$ | $6.03 \cdot 10^{5}$ | $\mathbf{1.43 \cdot 10^{-1}}$ | $3.00 \cdot 10^{-2}$ | $\mathbf{4.75 \cdot 10^{-8}}$ | $1.92 \cdot 10^{-9}$ |
| **IGF1R** | $\mathbf{4.76 \cdot 10^{5}}$ | $5.77 \cdot 10^{4}$ | $\mathbf{1.32 \cdot 10^{-1}}$ | $1.45 \cdot 10^{-2}$ | $\mathbf{2.78 \cdot 10^{-7}}$ | $1.95 \cdot 10^{-8}$ |
| **IKK-α** | $\mathbf{1.65 \cdot 10^{5}}$ | $2.91 \cdot 10^{3}$ | $\mathbf{1.48 \cdot 10^{-2}}$ | $3.10 \cdot 10^{-4}$ | $\mathbf{9.01 \cdot 10^{-8}}$ | $1.11 \cdot 10^{-9}$ |
| **IKK-β** | $\mathbf{3.16 \cdot 10^{5}}$ | $3.29 \cdot 10^{4}$ | $\mathbf{4.89 \cdot 10^{-2}}$ | $5.13 \cdot 10^{-3}$ | $\mathbf{1.54 \cdot 10^{-7}}$ | $7.85 \cdot 10^{-9}$ |
| **ITK** | $\mathbf{1.01 \cdot 10^{6}}$ | $8.06 \cdot 10^{4}$ | $\mathbf{7.77 \cdot 10^{-2}}$ | $6.80 \cdot 10^{-3}$ | $\mathbf{7.68 \cdot 10^{-8}}$ | $3.30 \cdot 10^{-9}$ |
| **JAK2** | $\mathbf{3.43 \cdot 10^{6}}$ | $7.05 \cdot 10^{4}$ | $\mathbf{1.36 \cdot 10^{-2}}$ | $3.20 \cdot 10^{-4}$ | $\mathbf{3.96 \cdot 10^{-9}}$ | $6.00 \cdot 10^{-11}$ |
| **KDR** | $\mathbf{1.44 \cdot 10^{5}}$ | $1.68 \cdot 10^{3}$ | $\mathbf{4.46 \cdot 10^{-3}}$ | $9.00 \cdot 10^{-5}$ | $\mathbf{3.09 \cdot 10^{-8}}$ | $4.40 \cdot 10^{-10}$ |
| **KIT** | $\mathbf{2.42 \cdot 10^{6}}$ | $1.19 \cdot 10^{5}$ | $\mathbf{2.00 \cdot 10^{-2}}$ | $1.12 \cdot 10^{-3}$ | $\mathbf{8.28 \cdot 10^{-9}}$ | $2.30 \cdot 10^{-10}$ |
| **LCK** | $\mathbf{1.58 \cdot 10^{6}}$ | $2.27 \cdot 10^{5}$ | $\mathbf{1.22 \cdot 10^{-1}}$ | $1.86 \cdot 10^{-2}$ | $\mathbf{7.73 \cdot 10^{-8}}$ | $3.58 \cdot 10^{-9}$ |
| **LYN A** | $\mathbf{2.27 \cdot 10^{6}}$ | $3.42 \cdot 10^{5}$ | $\mathbf{8.54 \cdot 10^{-2}}$ | $1.36 \cdot 10^{-2}$ | $\mathbf{3.76 \cdot 10^{-8}}$ | $1.63 \cdot 10^{-9}$ |
| **MAP2K1** | $\mathbf{1.71 \cdot 10^{5}}$ | $1.39 \cdot 10^{3}$ | $\mathbf{2.10 \cdot 10^{-4}}$ | $4.00 \cdot 10^{-5}$ | $\mathbf{1.23 \cdot 10^{-9}}$ | $2.30 \cdot 10^{-10}$ |
| **MET** | $\mathbf{2.57 \cdot 10^{5}}$ | $8.43 \cdot 10^{3}$ | $\mathbf{2.87 \cdot 10^{-2}}$ | $1.00 \cdot 10^{-3}$ | $\mathbf{1.12 \cdot 10^{-7}}$ | $1.57 \cdot 10^{-9}$ |
| **MPS1** | $\mathbf{1.16 \cdot 10^{6}}$ | $1.24 \cdot 10^{5}$ | $\mathbf{1.48 \cdot 10^{-1}}$ | $1.58 \cdot 10^{-2}$ | $\mathbf{1.28 \cdot 10^{-7}}$ | $2.79 \cdot 10^{-9}$ |
| **p38a** | $\mathbf{2.17 \cdot 10^{6}}$ | $2.63 \cdot 10^{5}$ | $\mathbf{8.99 \cdot 10^{-2}}$ | $1.11 \cdot 10^{-2}$ | $\mathbf{4.14 \cdot 10^{-8}}$ | $7.80 \cdot 10^{-10}$ |
| **PIK3CA** | $\mathbf{8.62 \cdot 10^{6}}$ | $1.74 \cdot 10^{5}$ | $\mathbf{4.98 \cdot 10^{-3}}$ | $1.60 \cdot 10^{-4}$ | $\mathbf{5.80 \cdot 10^{-10}}$ | $1.00 \cdot 10^{-11}$ |
| **PKCη** | $\mathbf{4.64 \cdot 10^{3}}$ | $8.77 \cdot 10^{1}$ | $\mathbf{3.04 \cdot 10^{-4}}$ | $1.00 \cdot 10^{-5}$ | $\mathbf{6.55 \cdot 10^{-8}}$ | $1.89 \cdot 10^{-9}$ |
| **PLK1** | $\mathbf{3.03 \cdot 10^{6}}$ | $2.75 \cdot 10^{5}$ | $\mathbf{1.95 \cdot 10^{-2}}$ | $1.94 \cdot 10^{-3}$ | $\mathbf{6.44 \cdot 10^{-9}}$ | $2.30 \cdot 10^{-10}$ |
| **RET** | $\mathbf{9.78 \cdot 10^{5}}$ | $2.88 \cdot 10^{4}$ | $\mathbf{7.40 \cdot 10^{-3}}$ | $2.90 \cdot 10^{-4}$ | $\mathbf{7.57 \cdot 10^{-9}}$ | $1.70 \cdot 10^{-10}$ |
| **ROCK1** | $\mathbf{9.21 \cdot 10^{4}}$ | $3.42 \cdot 10^{3}$ | $\mathbf{3.26 \cdot 10^{-2}}$ | $1.21 \cdot 10^{-3}$ | $\mathbf{3.54 \cdot 10^{-7}}$ | $8.44 \cdot 10^{-9}$ |
| **SRC** | $\mathbf{6.01 \cdot 10^{6}}$ | $2.26 \cdot 10^{6}$ | $\mathbf{1.69 \cdot 10^{-1}}$ | $6.48 \cdot 10^{-2}$ | $\mathbf{2.81 \cdot 10^{-8}}$ | $1.42 \cdot 10^{-9}$ |
| **Syk** | $\mathbf{2.73 \cdot 10^{6}}$ | $5.13 \cdot 10^{4}$ | $\mathbf{3.83 \cdot 10^{-3}}$ | $1.30 \cdot 10^{-4}$ | $\mathbf{1.40 \cdot 10^{-9}}$ | $4.00 \cdot 10^{-11}$ |
| **TGF-β1** | $\mathbf{2.10 \cdot 10^{6}}$ | $2.29 \cdot 10^{5}$ | $\mathbf{8.55 \cdot 10^{-2}}$ | $9.44 \cdot 10^{-3}$ | $\mathbf{4.06E \cdot 10^{-8}}$ | $7.10 \cdot 10^{-10}$ |
| **TIE2** | $\mathbf{2.43 \cdot 10^{6}}$ | $1.01 \cdot 10^{6}$ | $\mathbf{2.72 \cdot 10^{-1}}$ | $1.15 \cdot 10^{-1}$ | $\mathbf{1.12 \cdot 10^{-7}}$ | $6.21 \cdot 10^{-9}$ |
| **TRKB** | $\mathbf{7.68 \cdot 10^{6}}$ | $1.32 \cdot 10^{4}$ | $\mathbf{1.17 \cdot 10^{-3}}$ | $9.00 \cdot 10^{-5}$ | $\mathbf{1.52 \cdot 10^{-9}}$ | $1.10 \cdot 10^{-10}$ |

**Table S4. Related to all Figures and Tables:** Compounds screened in this study

| Compound name | CAS Number |
|---|---|
| 3-Methyladenine | 5142-23-4 |
| A66 | 1166227-08-2 |
| A-674563 | 552325-73-2 |
| A-769662 | 844499-71-4 |
| AEE788 (NVP-AEE788) | 497839-62-0 |
| Afatinib (BIBW2992) | 439081-18-2 |
| AG-1024 | 65678-07-1 |
| AG-1478 (Tyrphostin AG-1478) | 153436-53-4 |
| AG-490 | 133550-30-8 |
| AMG 900 | 945595-80-2 |
| AMG-208 | 1002304-34-8 |
| AMG458 | 913376-83-7 |
| Amuvatinib (MP-470) | 850879-09-3 |
| Apatinib (YN968D1) | 811803-05-1 |
| ARQ 197 (Tivantinib) | 905854-02-6 |
| ARRY334543 | 845272-21-1 |
| Arry-380 | 937265-83-3 |
| AS-252424 | 900515-16-4 |
| AS-604850 | 648449-76-7 |
| AS-605240 | 648450-29-7 |
| AS703026 (pimasertib) | 1236699-92-5 |
| AST-1306 | 1050500-29-2 |
| AT7519 | 844442-38-2 |
| AT7867 | 857531-00-1 |
| AT9283 | 896466-04-9 |
| Aurora A Inhibitor I | 1158838-45-9 |
| Axitinib | 319460-85-0 |
| AZ 960 | 905586-69-8 |
| AZ628 | 878739-06-1 |
| AZD2014 | 1009298-59-2 |
| AZD4547 | 1035270-39-3 |
| AZD5438 | 602306-29-6 |
| AZD6244 (Selumetinib) | 606143-52-6 |
| AZD7762 | 860352-01-8 |
| AZD8055 | 1009298-09-2 |
| AZD8330 | 869357-68-6 |
| AZD8931 | 848942-61-0 |
| Barasertib (AZD1152-HQPA) | 722544-51-6 |
| Baricitinib (LY3009104 - incb28050) | 1187594-09-7 |
| BEZ235 (NVP-BEZ235) | 915019-65-7 |
| BGJ398 (NVP-BGJ398) | 872511-34-7 |
| BI 2536 | 755038-02-9 |
| BI6727 (Volasertib) | 755038-65-4 |
| BIBF1120 (Vargatef) | 656247-17-5 |
| BIRB 796 (Doramapimod) | 285983-48-4 |
| BIX 02188 | 1094614-84-2 |
| BIX 02189 | 1094614-85-3 |
| BKM120 (NVP-BKM120) | 944396-07-0 |
| BMS 777607 | 1025720-94-8 |
| BMS 794833 | 1174046-72-0 |
| BMS-265246 | 582315-72-8 |
| BMS-599626 (AC480) | 714971-09-2 |

| Compound name | CAS Number |
|---|---|
| Bosutinib (SKI-606) | 380843-75-4 |
| Brivanib (BMS-540215) | 649735-46-6 |
| Brivanib alaninate (BMS-582664) | 649735-63-7 |
| BS-181 HCl | 1397219-81-6 |
| BX-795 | 702675-74-9 |
| BX-912 | 702674-56-4 |
| BYL719 | 1217486-61-7 |
| CAL-101 (GS-1101) | 870281-82-6 |
| CAY10505 | 1218777-13-9 |
| CCT128930 | 885499-61-6 |
| CCT129202 | 942947-93-5 |
| CCT137690 | 1095382-05-0 |
| Cediranib (AZD2171) | 288383-20-0 |
| CEP33779 | 1257704-57-6 |
| CH5424802 | 1256580-46-7 |
| CHIR-124 | 405168-58-3 |
| CHIR-98014 | 252935-94-7 |
| CI-1033 (Canertinib) | 267243-28-7 |
| CI-1040 (PD184352) | 212631-79-3 |
| CP 673451 | 343787-29-1 |
| CP-724714 | 537705-08-1 |
| Crenolanib (CP-868596) | 670220-88-9 |
| Crizotinib (PF-02341066) | 877399-52-5 |
| CX-4945 (Silmitasertib) | 1009820-21-6 |
| CYC116 | 693228-63-6 |
| Cyt387 | 1056634-68-4 |
| Dabrafenib (GSK2118436) | 1195765-45-7 |
| Dacomitinib (PF299804 - PF-00299804) | 1110813-31-4 |
| Danusertib (PHA-739358) | 827318-97-8 |
| Dasatinib (BMS-354825) | 302962-49-8 |
| DCC-2036 (Rebastinib) | 1020172-07-9 |
| Deforolimus (Ridaforolimus) | 572924-54-0 |
| Desmethyl Erlotinib (CP-473420) | 183320-51-6 |
| Dinaciclib (SCH727965) | 779353-01-4 |
| Dovitinib (TKI-258) | 405169-16-6 |
| Dovitinib Dilactic acid (TKI258 Dilactic acid) | 852433-84-2 |
| E7080 (Lenvatinib) | 417716-92-8 |
| ENMD-2076 | 1291074-87-7 |
| Enzastaurin (LY317615) | 170364-57-5 |
| Erlotinib HCl | 183319-69-9 |
| Everolimus (RAD001) | 159351-69-6 |
| Flavopiridol HCl | 131740-09-5 |
| Foretinib (GSK1363089 - XL880) | 849217-64-7 |
| GDC-0068 | 1001264-89-6 |
| GDC-0879 | 905281-76-7 |
| GDC-0941 | 957054-30-7 |
| GDC-0980 (RG7422) | 1032754-93-0 |
| Gefitinib (Iressa) | 184475-35-2 |
| Golvatinib (E7050) | 928037-13-2 |
| GSK1059615 | 958852-01-2 |
| GSK1070916 | 942918-07-2 |

| Compound name | CAS Number |
|---|---|
| GSK1120212 (Trametinib) | 871700-17-3 |
| GSK1838705A | 1116235-97-2 |
| GSK1904529A | 1089283-49-7 |
| GSK2126458 | 1086062-66-9 |
| GSK461364 | 929095-18-1 |
| GSK690693 | 937174-76-0 |
| Hesperadin | 422513-13-1 |
| HMN-214 | 173529-46-9 |
| IC-87114 | 371242-69-2 |
| Imatinib (Gleevec) | 152459-95-5 |
| Imatinib Mesylate | 220127-57-1 |
| IMD 0354 | 978-62-1 |
| INCB28060 | 1029712-80-8 |
| Indirubin | 479-41-4 |
| INK 128 (MLN0128) | 1224844-38-5 |
| JNJ-38877605 | 943540-75-8 |
| JNJ-7706621 | 443797-96-4 |
| Ki8751 | 228559-41-9 |
| KRN 633 | 286370-15-8 |
| Ku-0063794 | 938440-64-3 |
| KU-55933 | 587871-26-9 |
| KU-60019 | 925701-49-1 |
| KW 2449 | 1000669-72-6 |
| KX2-391 | 897016-82-9 |
| Lapatinib Ditosylate (Tykerb) | 388082-77-7 |
| LDN193189 | 1062368-24-4 |
| Linifanib (ABT-869) | 796967-16-3 |
| Linsitinib (OSI-906) | 867160-71-2 |
| LY2228820 | 862507-23-1 |
| LY2603618 (IC-83) | 911222-45-2 |
| LY2784544 | 1229236-86-5 |
| LY294002 | 154447-36-6 |
| Masitinib (AB1010) | 790299-79-5 |
| MGCD-265 | 875337-44-3 |
| Milciclib (PHA-848125) | 802539-81-7 |
| MK-2206 2HCl | 1032350-13-2 |
| MK-2461 | 917879-39-1 |
| MK-5108 (VX-689) | 1010085-13-8 |
| MLN8054 | 869363-13-3 |
| MLN8237 (Alisertib) | 1028486-01-2 |
| Motesanib Diphosphate (AMG-706) | 857876-30-3 |
| Mubritinib (TAK 165) | 366017-09-6 |
| Neratinib (HKI-272) | 698387-09-6 |
| Nilotinib (AMN-107) | 641571-10-0 |
| NU7441 (KU-57788) | 503468-95-9 |
| NVP-ADW742 | 475488-23-4 |
| NVP-BGT226 | 1245537-68-1 |
| NVP-BHG712 | 940310-85-0 |
| NVP-BSK805 | 1092499-93-8 |
| NVP-BVU972 | 1185763-69-2 |
| NVP-TAE226 | 761437-28-9 |
| ON-01910 | 1225497-78-8 |
| OSI-027 | 936890-98-1 |
| OSI-420 | 183320-51-6 |
| OSI-930 | 728033-96-3 |

| Compound name | CAS Number |
|---|---|
| OSU-03012 | 742112-33-0 |
| Palomid 529 | 914913-88-5 |
| Pazopanib HCl | 635702-64-6 |
| PCI-32765 (Ibrutinib) | 936563-96-1 |
| PD 0332991 (Palbociclib) HCl | 827022-32-2 |
| PD0325901 | 391210-10-9 |
| PD153035 HCl | 183322-45-4 |
| PD173074 | 219580-11-7 |
| PD318088 | 391210-00-7 |
| PD98059 | 167869-21-8 |
| Pelitinib (EKB-569) | 257933-82-7 |
| PF-00562271 | 939791-38-5 |
| PF-03814735 | 942487-16-3 |
| PF-04217903 | 956905-27-4 |
| PF-04691502 | 1013101-36-4 |
| PF-05212384 (PKI-587) | 1197160-78-3 |
| PH-797804 | 586379-66-0 |
| PHA-665752 | 477575-56-7 |
| PHA-680632 | 398493-79-3 |
| PHA-767491 | 845714-00-3 |
| PHA-793887 | 718630-59-2 |
| Phenformin HCl | 834-28-6 |
| PHT-427 | 1191951-57-1 |
| PI-103 | 371935-74-9 |
| Piceatannol | 10083-24-6 |
| PIK-293 | 900185-01-5 |
| PIK-294 | 900185-02-6 |
| PIK-75 | 372196-77-5 |
| PIK-90 | 677338-12-4 |
| PIK-93 | 593960-11-3 |
| PKI-402 | 1173204-81-3 |
| PLX-4720 | 918505-84-7 |
| Ponatinib (AP24534) | 943319-70-8 |
| PP-121 | 1092788-83-4 |
| PP242 | 1092351-67-1 |
| Quercetin (Sophoretin) | 117-39-5 |
| Quizartinib (AC220) | 950769-58-1 |
| R406 | 841290-81-1 |
| R406 (free base) | 841290-80-0 |
| R788 (Fostamatinib) | 901119-35-5 |
| R935788 (Fostamatinib disodium - R788 disodium) | 1025687-58-4 |
| Raf265 derivative | n.a.; Selleckchem Cat.No. S2200 |
| Rapamycin (Sirolimus) | 53123-88-9 |
| Roscovitine (Seliciclib - CYC202) | 186692-46-6 |
| Ruxolitinib (INCB018424) | 941678-49-5 |
| SAR131675 | 1433953-83-3 |
| Saracatinib (AZD0530) | 379231-04-6 |
| SB 202190 | 152121-30-7 |
| SB 203580 | 152121-47-6 |
| SB 216763 | 280744-09-4 |
| SB 415286 | 264218-23-7 |
| SB 431542 | 301836-41-9 |
| SB 525334 | 356559-20-1 |

| Compound name | CAS Number |
|---|---|
| SB590885 | 405554-55-4 |
| Semaxanib (SU5416) | 194413-58-6 |
| SGX-523 | 1022150-57-7 |
| SNS-032 (BMS-387032) | 345627-80-7 |
| SNS-314 | 1146618-41-8 |
| Sotrastaurin (AEB071) | 425637-18-9 |
| SP600125 | 129-56-6 |
| Staurosporine | 62996-74-1 |
| SU11274 | 658084-23-2 |
| Sunitinib Malate (Sutent) | 341031-54-7 |
| TAE684 (NVP-TAE684) | 761439-42-3 |
| TAK-285 | 871026-44-7 |
| TAK-733 | 1035555-63-5 |
| TAK-901 | 934541-31-8 |
| Tandutinib (MLN518) | 387867-13-2 |
| Temsirolimus (Torisel) | 162635-04-3 |
| TG 100713 | 925705-73-3 |
| TG100-115 | 677297-51-7 |
| TG101209 | 936091-14-4 |
| TG101348 (SAR302503) | 936091-26-8 |
| TGX-221 | 663619-89-4 |
| Thiazovivin | 1226056-71-8 |
| Tideglusib | 865854-05-3 |
| Tie2 kinase inhibitor | 948557-43-5 |
| Tivozanib (AV-951) | 475108-18-0 |
| Tofacitinib (CP-690550 - Tasocitinib) | 477600-75-2 |
| Tofacitinib citrate (CP-690550 citrate) | 540737-29-9 |
| Torin 1 | 1222998-36-8 |
| Torin 2 | 1223001-51-1 |
| TPCA-1 | 507475-17-4 |
| Triciribine (Triciribine phosphate) | 35943-35-2 |
| TSU-68 (SU6668) | 252916-29-3 |
| TWS119 | 601514-19-6 |
| Tyrphostin AG 879 (AG 879) | 148741-30-4 |
| U0126-EtOH | 1173097-76-1 |
| Vandetanib (Zactima) | 443913-73-3 |
| Vatalanib 2HCl (PTK787) | 212141-51-0 |
| Vemurafenib (PLX4032) | 918504-65-1 |
| VX-680 (MK-0457 - Tozasertib) | 639089-54-6 |
| VX-702 | 745833-23-2 |
| WAY-600 | 1062159-35-6 |
| WHI-P154 | 211555-04-3 |
| Wortmannin | 19545-26-7 |
| WP1066 | 857064-38-1 |
| WP1130 | 856243-80-6 |
| WYE-125132 | 1144068-46-1 |
| WYE-354 | 1062169-56-5 |
| WYE-687 | 1062161-90-3 |
| WZ3146 | 1214265-56-1 |
| WZ4002 | 1213269-23-8 |
| WZ8040 | 1214265-57-2 |
| XL147 | 956958-53-5 |
| XL-184 (Cabozantinib) | 849217-68-1 |
| XL765 | 1349796-36-6 |

| Compound name | CAS Number |
|---|---|
| Y-27632 2HCl | 129830-38-2 |
| YM201636 | 371942-69-7 |
| ZM 336372 | 208260-29-1 |
| ZM-447439 | 331771-20-1 |
| ZSTK474 | 475110-96-4 |

**Table S5. Related to Figures 3 and S4:** Area under the curve (AUC) and maximal target occupancy ($TO_{max}$) values for the simulated TO dynamics traces shown in Fig. 3c and Fig. S4d.

| Drug | Administration schedule | Kinase | AUC of TO trace simulated with PK-$K_D$ model | AUC of TO trace simulated with PK-BK model | Maximal TO for simulation with PK-$K_D$ model | Maximal TO for simulation with PK-BK model |
|---|---|---|---|---|---|---|
| **Dasatinib** | **1 mg/kg / 12h (day 3)** | **ABL** | 11.99 | 11.99 | 0.9997 | 0.9997 |
| | | **FYN** | 11.55 | 11.56 | 0.9880 | 0.9878 |
| | | **KIT** | 9.58 | 9.63 | 0.9237 | 0.9222 |
| | | **LCK** | 10.76 | 10.78 | 0.9650 | 0.9641 |
| | | **SRC** | 11.90 | 11.91 | 0.9970 | 0.9974 |
| | | **BTK** | 10.39 | 10.41 | 0.9530 | 0.9517 |
| **Dasatinib** | **1 mg/kg / 48h (day 7-8)** | **ABL** | 47.19 | 47.52 | 0.9996 | 0.9996 |
| | | **FYN** | 33.65 | 36.72 | 0.9862 | 0.9848 |
| | | **KIT** | 17.65 | 19.56 | 0.9126 | 0.9042 |
| | | **LCK** | 24.45 | 27.05 | 0.9590 | 0.9554 |
| | | **SRC** | 43.04 | 44.75 | 0.9970 | 0.9968 |
| | | **BTK** | 21.82 | 24.11 | 0.9450 | 0.9402 |
| **'Dasatinib-like' but clearance↑ (4x inter-compartmental CL; 10x plasma clearance)** | **0.2 mg/kg / 24h (day 3)** | **ABL** | 10.28 | 20.28 | 0.9920 | 0.9830 |
| | | **FYN** | 3.44 | 4.98 | 0.7742 | 0.6206 |
| | | **KIT** | 1.00 | 1.14 | 0.3343 | 0.1705 |
| | | **LCK** | 1.82 | 2.25 | 0.5320 | 0.3524 |
| | | **SRC** | 6.33 | 11.24 | 0.9430 | 0.8881 |
| | | **BTK** | 1.47 | 1.75 | 0.4550 | 0.2853 |
| **Ibrutinib (assuming** | **8 mg/kg / 24h** | **BTK** | 15.58 | 18.22 | 0.9953 | 0.9939 |
| | | **LCK** | 5.62 | 5.83 | 0.9343 | 0.9322 |

| | | | | | | |
|---|---|---|---|---|---|---|
| **kPCA $k_{off}$)** | **(day 4)** | **EGFR** | 12.74 | 14.22 | 0.9906 | 0.9894 |
| | | **ITK** | 3.34 | 5.54 | 0.8410 | 0.4785 |
| **Ibrutinib (assuming covalent binding)** | | **BTK** | - | 24.00 | - | 1.000 |
| | | **LCK** | - | 5.81 | - | 0.9326 |
| | | **EGFR** | - | 24.00 | - | 1.000 |
| | | **ITK** | - | 23.66 | - | 0.9877 |

**Table S6. Related to Figures 5 and S6:** Matched molecular pairs screened in this study

| | |
|---|---|
| Desmethyl Erlotinib<br>→ Erlotinib | 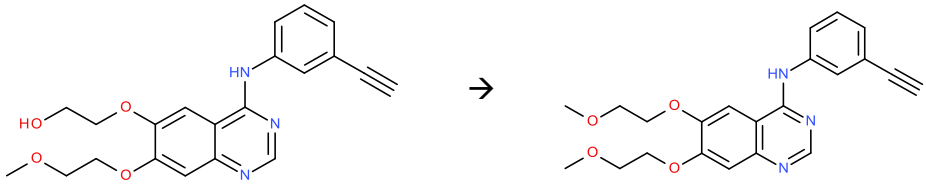 |
| PD153035<br>→ Tyrphostin AG-1478 | 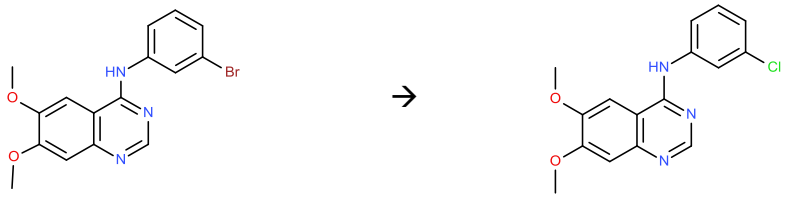 |
| WHI-P154<br>→ PD153035 |  |
| **BIX 02189**<br>**→ BIX 02188**<br>**($k_{on}$↑, $K_D$↓)** | 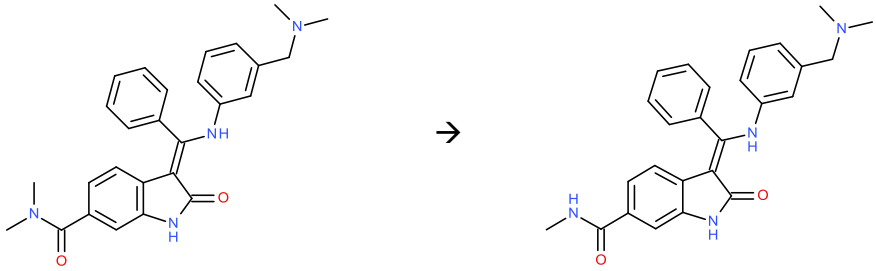 |
| Crenolanib<br>→ CP 673451<br>($k_{on}$↑, $k_{off}$↑) | 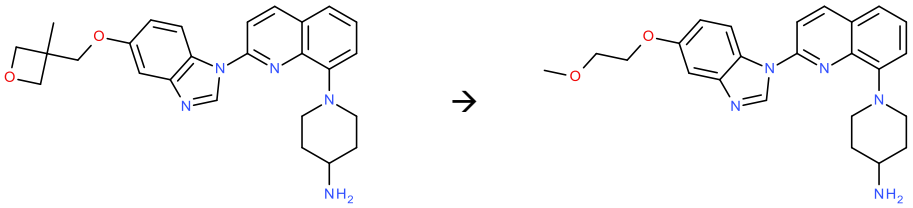 |
| **WZ4002**<br>**→ WZ3146**<br>**($k_{on}$↑, $K_D$↓)** | 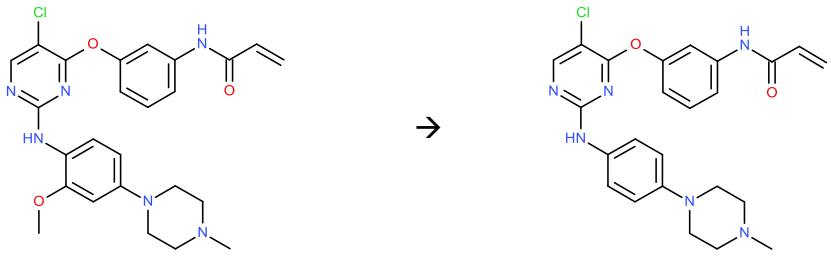 |

**Table S7. Related to Figures 5, 6, S6 and S7:** Comparison of quality of GFA models with 1) molecular properties as descriptors for binding parameters considering all kinase-inhibitor pairs, kinase-inhibitor pairs with $pK_D$ >8, or individual kinases (with $pK_D$ >8), 2) molecular properties or KLIFS binding mode information and/or KLIFS interaction fingerprints as descriptors for binding parameters (considering only kinase-inhibitor pairs with PDB and KLIFS entry). $r^2$ represents the percentage of variability of the data that can be described by the model.

| Comparison | $r^2$ of GFA model for | $\log(k_{on})$ | $-\log(k_{off})$ | $-\log(K_D)$ |
|---|---|---|---|---|
| 1 | **all kinase-inhibitor pairs** | 0.06 | 0.07 | 0.06 |
| | **all kinase- inhibitor pairs with $pK_D > 8$** | 0.16 | 0.16 | 0.06 |
| | **RET- inhibitor pairs with $pK_D > 8$** | 0.34 | 0.67 | |
| | **PIK3CA- inhibitor pairs with $pK_D > 8$** | 0.86 | 0.51 | |
| | **KDR- inhibitor pairs with $pK_D > 8$** | 0.30 | 0.45 | |
| | **AurA- inhibitor pairs with $pK_D > 8$** | 0.25 | 0.41 | |
| | **EGFR- inhibitor pairs with $pK_D > 8$** | 0.19 | 0.34 | |
| | **JAK2- inhibitor pairs with $pK_D > 8$** | 0.23 | 0.31 | |
| 2 | **Molecular properties** | 0.41 | 0.38 | 0.27 |
| | **KLIFS binding mode** | 0.43 | 0.33 | 0.15 |
| | **KLIFS interaction fingerprints** | 0.74 | 0.68 | 0.54 |
| | **KLIFS interaction fingerprints & molecular properties** | 0.79 | 0.69 | 0.58 |

SUPPLEMENTARY REFERENCES

(1) Wu, P.; Nielsen, T. E.; Clausen, M. H. *Trends Pharmacol Sci* **2015**, *36*, 422.